Unclassified

SECURITY CLASSIFICATION OF THIS PAGE

REPORT DOCUMENTATION PAGE

1a. REPORT SECURITY CLASSIFICATION UNCLASSIFIED	1b RESTRICTIVE MARKINGS
2a. SECURITY CLASSIFICATION AUTHORITY 2b. DECLASSIFICATION/DOWNGRADING SCHEDULE	3. DISTRIBUTION/AVAILABILITY OF REPORT Approved for public release; distribution is unlimited.
4. PERFORMING ORGANIZATION REPORT NUMBER(S)	5. MONITORING ORGANIZATION REPORT NUMBER(S)
6a. NAME OF PERFORMING ORGANIZATION Naval Postgraduate School 6b. OFFICE SYMBOL *(If applicable)* 31	7a. NAME OF MONITORING ORGANIZATION Naval Postgraduate School
6c. ADDRESS *(City, State, and ZIP Code)* Monterey, CA 93943-5000	7b. ADDRESS *(City, State, and ZIP Code)* Monterey, CA 93943-5000
8a. NAME OF FUNDING/SPONSORING ORGANIZATION 8b. OFFICE SYMBOL *(If applicable)*	9. PROCUREMENT INSTRUMENT IDENTIFICATION NUMBER
8c. ADDRESS *(City, State, and ZIP Code)*	10. SOURCE OF FUNDING NUMBERS Program Element No / Project No / Task No / Work Unit Accession Number

11. TITLE *(Include Security Classification)*
LIFT ENHANCEMENT USING A CLOSE-COUPLED OSCILLATING CANARD

12. PERSONAL AUTHOR(S) Schmidt, Dean C.

13a. TYPE OF REPORT	13b. TIME COVERED	14. DATE OF REPORT *(year, month, day)*	15. PAGE COUNT
Master's Thesis	From To	September 1992	118

16. SUPPLEMENTARY NOTATION
The views expressed in this thesis are those of the author and do not reflect the official policy or position of the Department of Defense or the U.S. Government.

17. COSATI CODES			18. SUBJECT TERMS *(continue on reverse if necessary and identify by block number)*
FIELD	GROUP	SUBGROUP	Oscillating, Dynamic Stall

19. ABSTRACT *(continue on reverse if necessary and identify by block number)*

A wind-tunnel study to investigate the effects of dynamic stall of a close-coupled canard on the canard/wing vortex interaction for increased lift enhancement was conducted. Two angles of attack of the model were studied: one at the first stall condition of the wing and one in the post-stall regime where a strong leading-edge vortex was formed. Baseline force and moment parameters were measured at mean canard deflections based on those determined to be optimum for the static case, as were mean values +/- 3 degrees about the optimum. The amplitude of oscillation considered was +/- 5 degrees about each mean; reduced frequencies tested were from 0.046 to 0.232. For most cases, lift was enhanced beyond the static-canard case at mean deflections equal to those at or greater than the static optimum value. The effective lift was decreased for mean deflections less than those previously determined to be optimum. Lift enhancements were generally 2 to 6 percent higher than the values determined with the static canard. The increased lift was generally independent of reduced frequency and peaked between k values of 0.1 to 0.2.

20. DISTRIBUTION/AVAILABILITY OF ABSTRACT ☒ UNCLASSIFIED/UNLIMITED ☐ SAME AS REPORT ☐ DTIC USERS	21. ABSTRACT SECURITY CLASSIFICATION Unclassified
22a. NAME OF RESPONSIBLE INDIVIDUAL Richard M. Howard	22b. TELEPHONE *(Include Area code)* 408-646-2870 22c. OFFICE SYMBOL AA/Ho

DD FORM 1473, 84 MAR 83 APR edition may be used until exhausted. All other editions are obsolete

SECURITY CLASSIFICATION OF THIS PAGE
Unclassified

Approved for public release; distribution is unlimited.

LIFT ENHANCEMENT USING A CLOSE-COUPLED OSCILLATING CANARD

by

Dean Christopher Schmidt
Lieutenant, United States Navy
B.S., United States Naval Academy, 1984

Submitted in partial fulfillment
of the requirements for the degree of

MASTER OF SCIENCE IN AERONAUTICAL ENGINEERING

from the

NAVAL POSTGRADUATE SCHOOL
September 1992

ABSTRACT

A wind-tunnel study to investigate the effects of dynamic stall of a close-coupled canard on the canard/wing vortex interaction for increased lift enhancement was conducted. Two angles of attack of the model were studied: one at the first stall condition of the wing and one in the post-stall regime where a strong leading-edge vortex was formed. Baseline force and moment parameters were measured at mean canard deflections based on those determined to be optimum for the static case, as were mean values ± 3 degrees about the optimum. The amplitude of oscillation considered was ± 5 degrees about each mean; reduced frequencies tested were from 0.046 to 0.232. For most cases, lift was enhanced beyond the static-canard case at mean deflections equal to those at or greater than the static optimum value. The effective lift was decreased for mean deflections less than those previously determined to be optimum. Lift enhancements were generally 2 to 6 percent higher than the values determined with the static canard. The increased lift was generally independent of reduced frequency and peaked between k values of 0.1 to 0.2.

TABLE OF CONTENTS

ACKNOWLEDGEMENTS

Completion of this work would not have been possible without the support of several individuals. I would like to acknowledge and personally thank each of them.

- Mr. Don Meeks designed and built the canard oscillating mechanism and provided the technical assistance which kept the model operating, despite several material failures, during testing.

- Mr. Ted Dunton graciously returned from retirement to repair the strain-gage balance and to provide technical training for NPS personnel.

- LCDRs James Clifton and Tom Stuart provided the necessary assistance and moral support which kept me going throughout the experiment.

- Professor Louis V. Schmidt monitored my progress in my advisor's absence. He provided the support and wisdom which enabled me to overcome several of the difficulties encountered during testing.

- Professor Richard M. Howard stuck by me during these last few months making himself available during all hours. His direction, guidence, and assistance in completing all aspects of this work is greatly appreciated.

Finally, I would like to acknowledge my wife, Judith, and my son, Christopher, for their patience during the last year.

Thanks, to you all!

I. INTRODUCTION

A. BACKGROUND

1. Agility

The design of fighter aircraft which exhibit a high level of agility continues to be of great importance even in today's environment of relaxed Superpower tensions. The definition of the term "agility" depends upon one's philosophical point of view. It can often be related to the terms, quick and nimble. McAtee states that "Agility is the capability to point the aircraft quickly and get the first shot; continue maximum maneuvering for self-defense and multiple kills; and accelerate quickly to leave the fight at will." [Ref.1] From a systems point of view, agility is "the ability of the entire weapon system to minimize the time delays between target acquisition and target destruction." [Ref.2] In simpler terms, aircraft agility can be described as "the time rate of change of the aircraft velocity vector." [Ref. 3] It can be seen that maneuverability and controllability are characteristics which are common to each of these views. Maneuverability may be described as the sum of forces acting on an aircraft which result in changes in airspeed and flight path, and controllability is essentially the ease with which the pilot changes flight path. [Ref. 1]

Historically, the importance of agility in war-fighting machines can be traced as far back as the year 1588 when Sir Frances Drake's nimble fleet of warships defeated the once invincible Spanish Armada, thus changing the course of European history and enabling the emergence of England as a colonial world power. Drake's ships carried no soldiers and were vastly out-gunned by the Spanish but they were able to out maneuver and wreak havoc on the Armada. [Ref. 4] An analogous process has been used in the design and utilization of fighter aircraft during the 20th century. Successful examples of such highly maneuverable aircraft from World Wars I & II and Korea include the Sopwith Camel, Supermarine Spitfire, ME-109, P-51 Mustang, and the F-86 Sabre. Each of these aircraft was able to take advantage of its inherent agility characteristics to achieve victory in aerial combat.

The advent of high agility aircraft such as the F-16, F-18, ATF, MIG-29 and SU-27 has meant that the maintenance of air superiority increasingly depends upon the ability of the fighter to rapidly point-and-shoot and to sustain increasingly high turn rates in air-to-air combat. This means that the modern fighter must be able to maneuver in the high angle-of-attack or even post-stall regime while at the same time, the aircraft must remain fully controllable. Accordingly, agility continues to be a predominant factor in evaluating the survivability and combat effectiveness of fighter aircraft. As aircraft engine and structural design engineers approach the limits of current technology, it becomes evident that they must seek new methods for squeezing increased performance from their designs.

2. Dynamic Stall

The dynamic stall phenomenon can be described as the unsteady motion of an airfoil or wing such as oscillations or a transient pitching motion which introduces significant vorticity in the flowfield that eventually coalesces into a dynamic stall vortex. Characteristically, dynamic stall occurs at angles of attack which greatly exceed those observed during static stall of the airfoil. As the airfoil is rapidly pitched upward, flow disturbances begin near the surface at the trailing edge and progress forward towards the leading edge. Then, at an angle of attack that depends on many parameters, a strong vortical flow develops near the leading edge of the airfoil. The vortex enlarges and moves down the airfoil inducing large excursions in lift and pitching moment. The additional lift generated due to unsteady motion is sustained as long as the vortex remains on the surface. As the angle of attack decreases (i.e. the airfoil is pitched downwards), the vortex moves into the wake and flow over the surface separates. [Ref. 5]

3. Supermaneuverability

Supermaneuverability is term which combines post-stall (PST) and direct force (DFM) capabilities. PST represents the ability of an aircraft to perform controlled maneuvers beyond maximum-lift angle of attack. DFM represents the ability of the aircraft to yaw and pitch independent of the flight path or to maneuver in roll and yaw at a constant fuselage attitude. PST may be used in aerial combat to trade energy for positional advantage. An aircraft which can execute a pitch-up maneuver to angles of attack as high as 90 degrees can complete a reversal of flight direction in approximately one-half the horizontal distance required for an aircraft limited to 20 degrees angle of attack. The supermaneuverable aircraft also completes this reversal in significantly less time than its adversary and thus has time to accelerate back to a high energy level. [Ref. 3]

4. Canard/Wing Interaction

Close-coupled canard/wing configurations have been in use for almost three decades. Properly spaced canard/wing planforms offer higher lift capabilities, enhanced maneuverability, and superior lift-to-drag ratios when compared to non-canard planforms. It is believed that constructive interference of the canard/wing vortex systems increases the maximum lift coefficient, and thus angle of attack, achievable by a close-coupled canard-configured aircraft. [Refs. 6 & 7]

5. Oscillating Canard Studies

Numerous studies of dynamic stall have been conducted using oscillating airfoils. Carr [Ref. 3] et al., provides a comprehensive review of the subject. However, little has been accomplished in the three-dimensional analysis. Several studies of three-dimensional oscillating wings have been conducted at the U.S. Air Force Academy. Using hot-wire anemometry, these experiments determined that the canard tip vortex had the greatest effect on the flow over a tandem wing and thus dominated the flowfield. No quantitative force-and-moment data were measured. Accordingly, conclusive evidence of positive effects on the wing was not achieved. [Refs. 8, 9 &10]

B. STATEMENT OF PURPOSE

Advancements in the field of high angle-of-attack maneuverability and controllability have the potential to create a lasting effect on the next generation of fighter aircraft. The purpose of this experiment was to investigate the phenomenon of dynamic stall as it applies to three-dimensional flow over an oscillating close-coupled canard and its interaction with the swept-wing vortex for a fighter configuration. It was desired to determine if the dynamic-stall vortex shed from the canard could provide an increased enhancement in the vortex coupling process. If the events which lead up to and follow the occurrence of dynamic stall can be fully understood and controlled, a superior fighter aircraft can be designed such that it can take full advantage of what is called "supermaneuverability". An initial step in understanding dynamic stall is being able to quantify its effects. In investigating the forces on a model undergoing canard oscillations, this experiment attempted to quantify the lift enhancement, or degradation, observed as the canard and swept-wing vortices interacted. Further, its purpose was to lay the ground work for further studies in this area based upon the experiment's successes or failures.

II. OBJECTIVES

A. BASELINE

The first goal of this experiment was to select two canard/wing model test conditions used by Kersh and verify his results. [Ref. 11] The data points which indicated the most improvement in lift qualities over a non-canard configuration were chosen. The first was a case with the model placed at 22 degrees angle of attack and the canard at +7 degrees deflection, for which a 34-percent increase in maximum lift coefficient was observed. For this case, the canard vortex served to reattach the wing flow at the first stall condition. A second baseline configuration was selected with the model placed at 34 degrees angle of attack and the canard deflected -7 degrees. An improvement of 9.4-percent in lift coefficient was seen for this configuration, which was the regime where a strong leading-edge vortex had formed. It was determined that fixed-canard lift and drag measurements would be made at these configurations and that the canard deflection would be varied $\pm$ 3 degrees (i.e. Alpha = 22 deg. with Deltac = +4, +7, +10 deg. and Alpha = 34 deg. with Deltac = -4, -7, -10 deg.) to provide a range of mean values around which to oscillate the canard.

B. EFFECTS OF CANARD OSCILLATION

The canard section was fitted with an electric motor and oscillation mechanism which was connected to the canard pivot point located at 40 percent of its exposed root chord. Once the fixed-canard lift and drag characteristics were obtained, the canard was configured for oscillation. The objective was to oscillate the canard about the above mean deflection angles at frequencies ranging from 5 to 25 hertz. Data was to be presented in the non-dimensional coefficients, C_L and k. C_L represents the lift coefficient and k represents reduced frequency. The following equation was used for the calculation of reduced frequency:

$$k=\frac{(\omega*(MAC/2))}{V} \tag{1}$$

Where:

ω	-	Frequency (radians/second)
MAC	-	Canard mean aerodynamic chord (5.38 inches)
V	-	Freestream velocity (ft/sec)

Lift and Drag data was to be obtained at oscillation amplitudes of $\pm$ 5 degrees and $\pm$ 10 degrees. It was desired to ascertain the effects of varied oscillation frequencies and amplitudes on the resultant enhanced lift.

III. EXPERIMENTAL APPARATUS

A. WIND TUNNEL

The Naval Postgraduate School (NPS) horizontal low-speed wind tunnel was used for the experiment. Figure 1 shows a diagram of the NPS low-speed wind tunnel. The tunnel is powered by a 100 HP electric motor connected to a standard four-speed truck transmission which turns a three-blade variable-pitch fan. The tunnel is of the single-return type. Airflow is straightened by a set of stator blades immediately aft of the fan. Ambient turbulence intensity in the tunnel test section is about 0.2%. The tunnel's contraction ratio (ratio of cross-section areas between the settling section and test section) of 10:1 combined with fine wire mesh screens at the entrance to the settling chamber contribute to the reasonable value of the test-section turbulence level. The tunnel test section measures 45 inches wide by 32 inches high. Lighting and a reflection plane in the test section reduce the tunnel height to 28 inches and the corresponding effective cross-sectional area to 9.88 square feet. The tunnel is equipped with an external flush-mounted cylindrical strain-gage reflection-plane (wall) balance which is attached to a remotely-controlled turntable. Four four-arm strain-gage bridges separated by 26.5 inches were used to measure axial and normal forces. A more complete

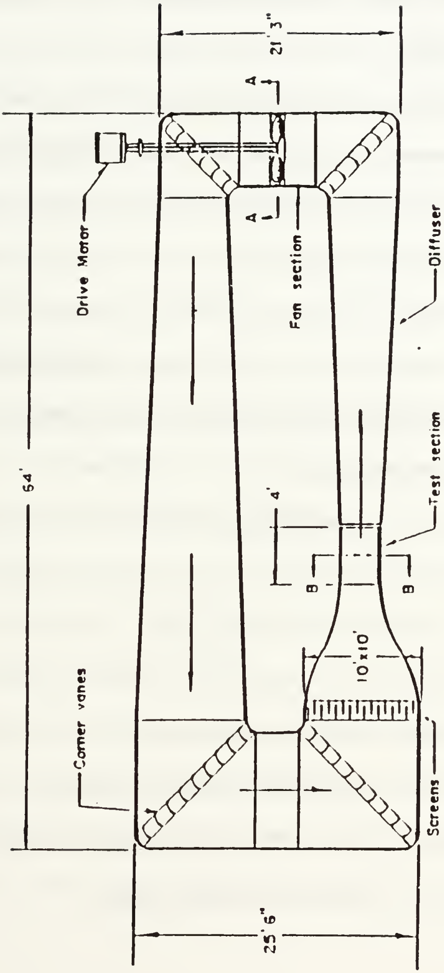

Figure 1: NPS Low-Speed Wind Tunnel

discussion of the balance is given in Section C. The turntable allowed for a variation of the model angle of attack. The temperature of the tunnel air was measured with a dial thermometer mounted on the tunnel wall extending into the settling chamber.

Test section dynamic pressure, q, was determined by measuring the pressure difference, ΔP, between the test section and the settling chamber static pressures using a water manometer. The settling chamber and the test section each have four wall-mounted static pressure taps that are connected to the manometer via a common manifold. The pressure difference measured by the manometer, in centimeters of water, was converted to the test section dynamic pressure and test section reference velocity using a previous tunnel calibration. Equations (2) and (3) show these relationships.

$$q = 2.047 * (-0.026749 + 1.1149 * \Delta P) \tag{2}$$

$$V = \sqrt{\frac{q}{\frac{1}{2} * \rho}} \tag{3}$$

Where:

- ρ - Density of air (slugs/ft^3)
- ΔP - Manometer reading in cm of H_2O
- q - Test section dynamic pressure (lbf/ft^2)
- V - Reference velocity (ft/sec)

The wind tunnel calibration factor, 1.1149, and tunnel calibration intercept, - 0.0267649, corrected the manometer reading, ΔP, to the test section dynamic pressure. The calibration factor was found by plotting the actual dynamic pressure measured by a pitot static tube mounted in the test section versus the measured pressure difference. The relationship was found to be linear, with the slope of the curve being the tunnel calibration factor. The slope did not pass through the origin, which resulted in there being a tunnel calibration intercept with the y-axis. [Refs. 11 &12]

B. CANARD/ WING MODEL

The canard/wing model was a half-body model fabricated from mahogany. It was designed to be compatible with the existing reflection-plane balance installed in the wind tunnel. The model was a generic fighter fuselage with a low-aspect-ratio close-coupled canard and wing. The canard and wing surfaces were wood reinforced with aluminum cores. The model consisted of three main sections: an ogive nose, a mid-section with canard, and an aft section with the wing mounted. The ogive nose section was permanently attached to the aluminum base. The removable canard section housed an electric motor and a sending unit used for measuring the canard oscillation frequency. The removable aft section provided support for the mid-section and a path for power and sensor cables to follow within the model. The model angle of attack was varied using the tunnel turntable. Figure 2 is a sketch of the model. Appendix A contains a detailed description of the model and the design process. [Ref. 11]

C. BALANCE AND TURNTABLE

The external strain-gage balance and turntable, Figure 3, mounted in the horizontal low-speed wind tunnel, was originally built by NPS personnel in 1974. It was designed to measure normal and axial forces and pitching moment in the wind tunnel. The balance itself was capable of measuring forces of up to 150 lbf. Each of the four external strain-gage bridge circuits had four active legs for automatic temperature compensation. The normal and axial moments were measured by two orthogonal strain-gage bridges cemented on balance column flexure links at two axial stations separated by a vertical distance of 26.5 inches. With the wind tunnel in operation, the force on the model created different moments on the upper and lower strain-gage bridges. The voltage signals from the four bridge circuits were converted to axial and normal forces using the results of a balance calibration, described in Appendix B. The balance column was rigidly mounted on an electrically-controlled turntable capable of rotating from -18 to +200 degrees relative to the tunnel centerline. The model was mounted on top of an aluminum turntable disk which was flush with the reflection plane. A one-eighth

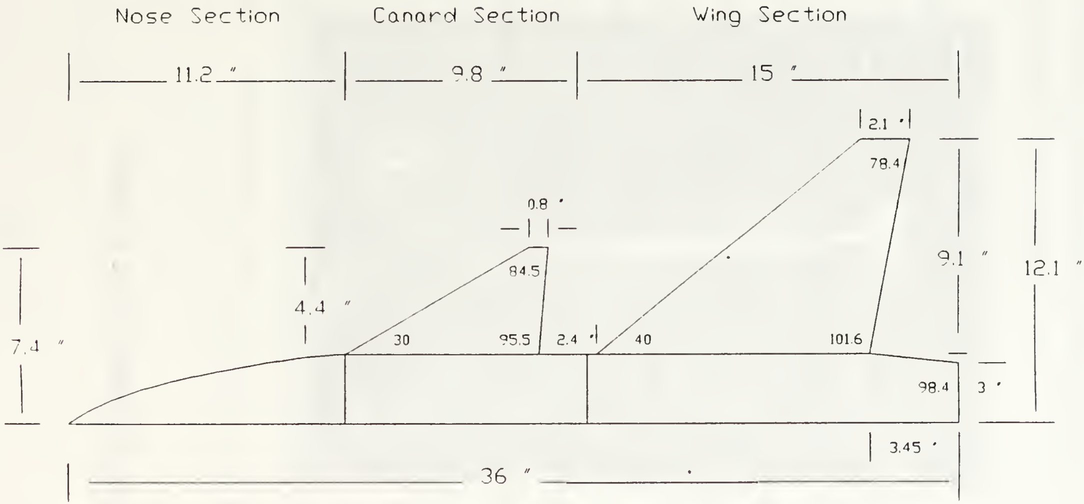

Figure 2. Canard/Wing Half-Body Model

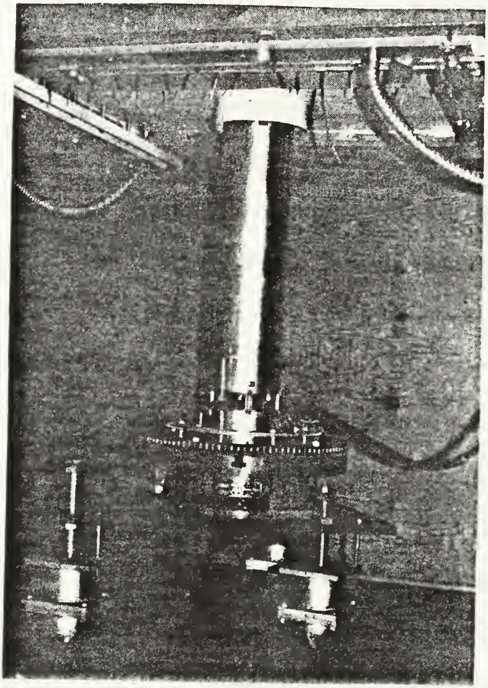

Figure 3. Strain-gage Balance and Turntable

inch gap existed between the turntable disk and the reflection plane. This gap isolated the model and wall balance from the reflection plane in order to preserve integrity of the wall balance load readings.

D. DATA ACQUISITION HARDWARE AND SOFTWARE

Each strain-gage bridge had an individual signal conditioning assembly that supplied the excitation voltage. The signal conditioning assemblies allowed their associated strain-gage bridges to be zeroed and calibrated. The signal from each conditioner was passed through a Pacific® 8255/6 low-noise amplifier with the gain set at 1000. Signals were processed by a National Instruments® MC-MIO-16L-9 12-bit multi-function board as inputs to an IBM PS/2® computer. The MC-MIO-16L-9 has an Analog-to-Digital (A/D) converter with a 9 μsec. conversion time and is capable of data acquisition rates of up to 100 Kbytes/sec. The board's digitation span was 4096 bits (i.e. 2^{12} bits), giving a resolution of the analog-to-digital conversion of 4.88 mvolts. [Ref. 19] A Microsoft QuickBasic 4.5® program which implemented MC-MIO-16-9 board commands for data acquisition was compiled. The program was written with the help of National Instruments LabWindows® interactive software. A complete listing of the code can be found in Appendix D.

IV. EXPERIMENTAL PROCEDURES

A. CALIBRATION

1. Signal Conditioning

Figure 4 illustrates the calibration rig. The rig was mounted directly to the tunnel reflection plane. Axial line up was accomplished visually. The turntable vernier was then adjusted to zero so that all direct angle readings would be accurate. The height of the cable attachment was adjusted to either 10.5625 inches or 7.75 inches above the floor of the reflection plane, depending upon which calibration run was being conducted. A bubble level was used to adjust the pulley height so that the loading cable was horizontal. Load application to the wall balance using the calibration frame resulted in voltages being processed by the amplifiers. Prior to taking voltage readings, the amplifiers were adjusted for gain and zero offsets. While the inputs to the Pacific® 8255/6 operational amplifiers were shorted and the gain was set to 1, the output set screw was adjusted to produce a reading of 0 ± 100 μvolts. The gain was then set to 1000 and the input set screw was adjusted to obtain a reading of 0 ± 500 μvolts. The amplifier shorts were then removed and the signal conditioners were set to a bridge span of 10 ± 0.05 volts and zeroed to 0 ± 0.05 volts. As zeroing the signal conditioners

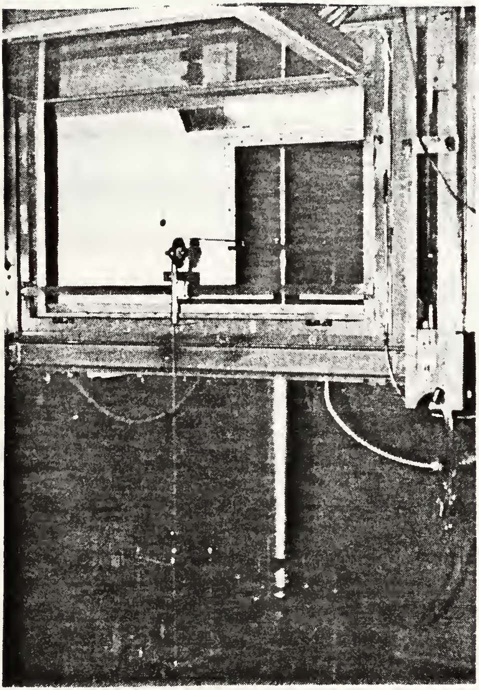

Figure 4. Calibration Rig

exactly was difficult, it was determined that the data acquisition program would be written so as to note voltage offsets or tare readings and automatically adjust for them during data reduction.

2. Equipment Failure

Initial calibration efforts using the Hewlett-Packard® Panels program indicated numerous problems in accuracy and repeatability. As with any strain-gage installation, it was expected that difficulties would generally fall into one of three categories: (1) wire connections, (2) thermal expansion, (3) and moisture absorption. [Ref. 13] The latter two problems were deemed to be negligible as there was little temperature variation during the calibration and virtually no moisture in the tunnel area. Thus, all cannon plugs and wire connections from the cylindrical wall balance through the signal conditioners and operational amplifiers were inspected, cleaned and tightened where necessary. Finally, inspection of the strain-gage bridges themselves led to the source of the inaccuracies. It was determined that the strain gage at position J of Figure B3 (Appendix B) had separated from the cylinder wall thus making all readings erroneous. Further, it was noted that the balance flexures on the cylinder, where the strain-gages were mounted, had buckled in several places. This was apparently due to misuse of the balance over a long period of time. With some difficulty (see Acknowledgements), the strain-gage was replaced and calibration was again commenced. Unfortunately, the Hewlett Packard® Digital Multi-Meter data acquisition system failed at this time. With no replacement and an unspecified time required for repair, a new method of data acquisition was necessary. With this in mind, the IBM PS/2® computer and National Instruments® MC-MIO-16L-9 multi-function board system in the NPS vertical low-speed wind tunnel was considered for use. The board, along with its LabWindows® interactive software, was functionally tested in the vertical wind tunnel area, then moved to the horizontal low-speed wind tunnel for data acquisition. Electrical noise became a problem as several Pacific® 8255/6 operational amplifiers were tested before satisfactory results were achieved. Appendix B illustrates the calibration process.

3. Data Acquisition

Approximately 100 data points were taken for each height and direction. Each data point was the mean of 1000 voltage readings taken over the span of 2.25 seconds. The corresponding data acquisition rate was 444.44 hertz. The resulting maximum on-axis standard error of regression was less than 0.3 percent. Deflection of the horizontal bar which supported the pulley limited the calibration loading to 35.2 lbf when the cable height was 10.5625 inches and to 55.2 lbf. when the height was 7.75 inches. The maximum loads expected during tunnel operation were approximately 50 lbf. The calibration data indicated that strain-gage response was linear throughout the range of loading. The strain-gage response was assumed to be linear within the structural limits of the balance. The calibration data is included in Appendix B.

B. BASELINE VALIDATION

The experiment was initiated as a follow-on to previous NPS wind tunnel work which studied lift enhancement using close-coupled canard/wing vortex interaction with a static canard. [Ref. 11] As a result, a test objective was to keep the following parameters constant:

1. Test Section ΔP = 17 cm H_2O
2. Test Section Velocity = 172 ft/sec.
3. Reynolds Number = 9.5×10^5, Ref. to wing MAC

In the study by Kersh, the most profound positive effects of canard/wing vortex interaction were found to occur at angles of attack where major flow separation existed. In this regime, the enhanced lift was thought to be the result of constructive interference of the canard and wing vortical flowfields.

Nineteen wind-tunnel runs were made to validate the procedures and the baseline data. A checklist of procedures was created to ensure that test conditions remained constant. The steps for each tunnel run were as follows:

1. Tunnel Temperature and pressure was recorded.
2. H_2O manometer was zeroed.
3. Model angle of attack zeroed, then set to desired angle.
4. Canard incidence set, oscillation amplitude set (if required).
5. Operational Amplifiers zeroed.
6. Signal Conditioners zeroed and span set.

7. Tare voltage readings taken and checked constant within 0.01 lbf.

8. Mark time.

9. Turn tunnel on and set to ΔP = 17 cm. H_2O.

10. Supply power to canard, set oscillation frequency (if required).

11. Record five readings of voltage for each test condition, check manometer and oscillation frequency between each set.

12. Secure tunnel.

13. Check for voltage drift when tunnel fully stopped.

14. Mark time.

Analysis of initial test runs indicated that the balance calibration procedure was correct and the load values previously obtained were repeatable if the unloaded signal drift was subtracted from all readings. As in the calibration process, each data point was the average of 1000 voltage readings taken over the span of 2.25 seconds. In an effort to determine the source of the drift, the signal variance from the balance signal was checked with the model removed and the tunnel at zero airspeed over a period of one hour. The signal was then checked with the model removed and the tunnel operating at the desired airspeed over a period of fifteen minutes. In both cases, the signal drift was negligible. Test runs were subsequently made with the model at 22 degrees angle of attack and the canard fixed at +4, +7, and +10 degrees deflection. The model was then configured for canard oscillation. Numerous wind tunnel runs indicated that the electric motor was unable to overcome the dynamic pressure on the canard at ΔP = 17 cm. The canard was designed to pivot about its 40 percent exposed root chord position which was physically located 3.2 inches aft of the leading edge at the root. This position corresponded to 7 percent of the mean aerodynamic chord. The canard's 25 percent mean aerodynamic chord position was located 4.15 inches aft of the leading edge. This aerodynamic loading was assumed to be the primary cause of the motor's failure to oscillate the canard.

Experimental runs were then conducted to determine a manometer setting which would allow canard oscillation. A value of ΔP = 12 cm. was chosen and was held constant for the remainder of the experiment.

C. DATA COLLECTION

The new test objective was to keep the following parameters constant:

1. Test Section ΔP = 12 cm. H_2O
2. Test Section Velocity = 150 ft/sec.
3. Reynolds Number = 7.7×10^5, Ref. to wing MAC

The baseline procedures stated above were repeated for each tunnel run. The model was initially placed at 22 degrees angle of attack. Lift and drag measurements were obtained with the canard fixed at +4, +7, and +10 degrees deflection. The test were repeated with the model at 34 degrees angle of attack and the canard fixed at -4, -7, and -10 degrees deflection. The canard section of the model was then removed and the internal mechanism was adjusted to achieve an oscillation amplitude of ± 5 degrees. The model was then reinstalled and tests were conducted under the above conditions with the canard oscillating. Once the tunnel was stabilized at 12 cm H_2O, the DC power supply was energized and adjusted to achieve the desired frequency of oscillation. A sending unit mounted inside the canard section counted the teeth of a sprocket attached to the motor's shaft as it rotated. The instantaneous count per second was displayed on a Fluke® 7250A universal counter/timer. Frequency was calculated by dividing the displayed count by the number of teeth on the sprocket. During each run, frequency was varied from 5 to 25 hertz in increments of 5 hertz. This corresponded to reduced frequencies ranging from 0.046 to 0.232. Five readings were taken at each point. The tunnel was secured and the entire process was repeated two more times to ensure that the results could be duplicated. The canard was then adjusted for a ±10-degree amplitude of oscillation. Tests were then attempted at the above model settings. It was found that the frequency could not be controlled below 10 hertz and that the power supply could not provide enough voltage to stabilize the frequency at 25 hertz. Further, it became obvious that the set screws which secured the canard to the shaft of the motor were loosening during each run. Finally, the pin which secured the canard at the pivot point sheared during a tunnel run. The pin was repaired but the canard remained loose at the pivot point and the shaft connection continued to loosen during test runs. Due to time constraints, the test was terminated at this point. The experimental data is enclosed in Appendix E. A summary of the results and discussion is included in Chapter V.

V. RESULTS AND DISCUSSION

The following section presents the results of 52 wind tunnel runs and a total of 259 minutes of testing. Baseline values of lift and drag were obtained with the tunnel set at ΔP = 17 cm H_2O and canard incidence fixed at several positions. The model was first placed at 22 degrees angle of attack and tunnel runs were made with the canard fixed at +4, +7, and +10 degrees deflection relative to the model's centerline. This angle of attack and the canard deflection angles were chosen for comparison with previous work which showed a 34-percent lift improvement over a non-canard configured model at 22 degrees angle of attack with +7 degrees canard deflection. [Ref. 11] The gear mechanism attached to the electric motor inside the canard section of the model was then adjusted to create a canard deflection amplitude of $\pm$ 5 degrees during oscillation. The canard was then oscillated at frequencies varying from 5 to 25 hertz and corresponding reduced frequencies from 0.046 to 0.232. For comparison to fixed-canard data, the canard was set at mean deflection angles of +4, +7, and +10 degrees. It was found that electric motor which was oscillating the canard could not provide enough power to overcome the aerodynamic forces encountered at this dynamic pressure setting. A new baseline at ΔP = 12 cm H_2O was chosen so that fixed-canard and oscillating-canard data could be directly compared. The data for the fixed-canard configurations at ΔP = 17 cm H_2O were kept for comparison with previous work and are enclosed in Appendix F. The above procedures for the model at 22 degrees angle of attack were repeated at the new manometer setting. The model was then set to 34 degrees angle of attack and tunnel runs were made with the canard deflection fixed at -4, -7, and -10 degrees. Previous work had indicated that a 9.4-percent lift improvement over a non-canard configuration occurred at this angle of attack and -7 degrees canard deflection. [Ref. 11] The tunnel tests were then repeated with the canard oscillating about mean deflection values of -4, -7, and -10 degrees. C_L and C_D represent the lift and drag coefficients and were obtained from at least ten recordings. The following equations were used for their calculation:

$$C_L = \frac{Lift}{(q*S)} \tag{4}$$

$$C_D = \frac{Drag}{(q*S)} \tag{5}$$

Where:

Lift, Drag	-	Force (lbf)
q	-	Dynamic Pressure (lbf/ft^2)
S	-	Reference Area of exposed canard and wing (0.815 ft^2)

A. ALPHA = 22 DEGREES

At this angle of attack, Kersh found that the lift coefficient increased as the fixed canard deflection angle was varied from 0 to +7 degrees. In this regime, the canard/wing vortex interaction had a positive effect on the flowfield as flow separation, and thus stall, was delayed. Above +7 degrees canard deflection, flow separation on the upper surface of the wing overcame the positive effects of the canard's shed vortex. Lift coefficient then began to taper off. The canard deflection angles of +4, +7, and +10 degrees were chosen for this experiment in order to verify these results and determine the effect of oscillations at and near the optimum fixed-canard deflection angle. Frequencies of 5 to 25 hertz (k = 0.046 to 0.232) were selected in an effort to quantify their effects. Canard amplitude variations of ± 5 degrees and ± 10 degrees were selected for comparison purposes. However, the model was unable to function properly at the ± 10 degree amplitude. Data was only obtained in the ± 5 degree configuration. Figure 5 shows the variation of mean C_L with reduced frequency at this angle of attack and canard mean deflection angles of +4, +7, and +10 degrees. The error bars represent the root-mean-squared (R.M.S.) error of the data. The largest scatter in the data was observed at the reduced frequency of 0.046. It is assumed that this was due to the difficulties encountered in stabilizing the power supply's voltage and thus, the canard's frequency at this low setting.

1. Canard Deflection = +4 Degrees

The canard's mean angle of attack was 26 degrees. Figure 5 shows that the maximum lift coefficient in this configuration was achieved when the canard was fixed. At k = 0.232, the lift coefficient was 6.8 percent less than the fixed-canard value. Although the fixed canard was at a deflection angle below that for the maximum-lift angle of attack, the introduction of unsteady flow resulted in a loss of lift. The vortex shed from the canard surface during the dynamic stall occurrence negated the previous improvements seen with a fixed canard. Table 1 lists the frequency, mean lift coefficient and mean drag coefficient for this configuration.

TABLE 1: ALPHA = 22, DELTAC = +4

Hertz	0	5	10	1[illegible]	20	25
k	0.000	0.046	0.093	0.139	0.186	0.232
Mean CL	1.2240	1.1657	1.1685	1.1657	1.1547	1.1406
Mean CD	0.4603	0.4519	0.4495	0.4449	0.4433	0.4380

2. Canard Deflection = +7 Degrees

The figure shows that the maximum lift coefficient during this portion of the experiment was achieved at the reduced frequency of 0.139. This increase was a 2.6 percent gain over that of the fixed-canard configuration. The canard was at a mean value of 29 degrees angle of attack during this phase, the value representing the peak of the lift curve slope when the canard was fixed. The positive effects of oscillation began to taper off as frequency was further increased. Table 2 shows the data for the model at 22 degrees angle of attack and canard at +7 degrees deflection.

TABLE 2: ALPHA = 22, DELTAC = +7

Hertz	0	5	10	15	20	25
k	0.000	0.046	0.093	0.139	0.[illegible]86	0.232
Mean CL	1.2720	1.2902	1.3028	1.3052	1.3042	1.2928
Mean CD	0.4808	0.4840	0.4850	0.4839	0.4805	0.4776

3. Canard Deflection = +10 Degrees

The positive effects of the canard/wing vortex interaction in the fixed-canard configuration diminished as deflection was increased beyond +7 degrees. At +10 degrees deflection, the canard was at 32 degrees mean angle of attack. Figure 5 shows that the introduction of unsteady flow to this flowfield resulted in a 6 percent increase in lift coefficient for all frequencies tested. This increase was significantly greater than that observed when the mean canard deflection was +7 degrees. It is thought that the stronger vortex shed from the canard at this angle of attack resulted in the greater lift enhancement. Table 3 shows the reduced data for this configuration.

TABLE 3: ALPHA = 22, DELTAC = +10

Hertz	0	5	10	15	20	25
k	0.000	0.046	0.093	0.093	0.186	0.232
Mean CL	1.1654	1.2072	1.2317	1.2316	1.2389	1.2345
Mean CD	0.4728	0.4833	0.4869	0.4852	0.4853	0.4822

B.   ALPHA = 34 DEGREES

Kersh's work indicated that the lift coefficient increased as the fixed-canard deflection angle was varied from 0 to -7 degrees, at this angle of attack. In this regime, the canard/wing vortex interaction had a positive effect on the flowfield as flow separation, and thus stall, was delayed. At canard deflection angles less than -10 degrees (i.e. more negative), the canard vortex was less effective in providing a positive interaction with the flow over the wing. As a follow-on, canard deflection angles of -4, -7, and -10 were selected for comparison purposes at and near the fixed-canard peak lift angle of attack. The frequencies and amplitude stated above were also used. Oscillating the canard with the model at 34 degrees angle of attack produced effects which differed from those seen at 22 degrees angle of attack. Flow separation along the wing's upper surface was stronger at the higher angle of attack. This flow characteristic apparently delayed the onset of lift enhancement until the canard mean angle of attack was greater than that for maximum fixed-canard lift enhancement. Figure 6 illustrates the variation of mean C_L with reduced frequency at 34 degrees angle of attack. The maximum R.M.S. error observed was less than 1 percent.

1. Canard Deflection = -4 Degrees

The mean canard angle of attack was 30 degrees during these runs. When the canard was fixed, the model was experiencing the onset of stall and a diminishing of maximum available lift. The introduction of oscillations positively effected the vortical flow over the wing surface. As can be seen in Figure 6, a 3-percent increase in lift was seen at all frequencies. Maximum lift coefficient was achieved at the reduced frequency of 0.154. Table 4 summarizes the lift and drag data for this deflection angle.

TABLE 4: ALPHA = 34, DELTAC = -4

Hertz	0	5	10	15	20	25
k	0.000	0.046	0.093	0.139	0.[illegible]86	0.232
Mean CL	1.4785	1.5260	1.5289	1.5289	1.5222	1.5258
Mean CD	0.9052	0.9261	0.9256	0.9245	0.9211	0.9236

2. Canard Deflection = -7 Degrees

This deflection produced a canard angle of attack of 27 degrees. Figure 6 shows that the maximum lift coefficient attained was in the fixed-canard configuration. The introduction of unsteady flow over the wing surface reduced the model's lift by 1.7 percent. At this model angle of attack, the upper surface of the wing was experiencing severe flow separation. The strength of the vortex shed from the canard during oscillation was insufficient to reattach the flow. The positive effects obtained during steady flow were no longer achievable. Table 5 shows the reduced data for this configuration.

TABLE 5: ALPHA = 34, DELTAC = -7

Hertz	0	5	10	15	20	25
k	0.000	0.046	0.093	0.139	0.186	0.232
Mean CL	1.5124	1.4868	1.4908	1.4869	1.4907	1.4897
Mean CD	0.9130	0.8993	0.8987	0.8957	0.8975	0.8998

3. Canard Deflection = -10 Degrees

The canard angle of attack was 24 degrees. A relatively weak vortex was shed from the canard's leading edge during oscillations. The flowfield was dominated by separation along the wing's upper surface. This produced a negative effect on the model's lift capability, as depicted in Figure 6, as lift coefficient was reduced by 7.2 percent. Table 6 shows the reduced data for this configuration.

TABLE 6: ALPHA = 34, DELTAC = -10

Hertz	0	5	10	15	20	25
k	0.000	0.046	0.093	0.139	0.186	0.232
Mean CL	1.5012	1.4161	1.4088	1.3995	1.3935	1.4176
Mean CD	0.8887	0.8266	0.8218	0.8159	0.8125	0.8323

C. SUMMARY OF RESULTS

Figures 7 and 8 compare the fixed-canard lift characteristics with those of the canard oscillating at k = 0.139. These plots illustrate several of the effects of inducing dynamic stall on the canard. It can be seen that the introduction of unsteady flow over the canard at a deflection less than that for maximum lift enhancement had a negative effect. In the regime which was very close to and beyond canard deflection for maximum lift enhancement, canard oscillation had a positive effect. In this area, maximum lift coefficient was increased and the corresponding angle of attack was greater than that of the fixed canard.

Lift enhancement began at different canard angles of attack relative to the fixed-canard angle of attack for maximum lift enhancement. The positive effects began one degree prior to the canard deflection for maximum lift enhancement for the model at 22 degrees. These effects were delayed until one degree after this angle when the model was at 34 degrees. This is thought to be a result of the relative strength of the flow separation along the upper surface of the wing. It is evident that the dynamic stall phenomenon increased the available stall angle of attack and the maximum lift coefficient.

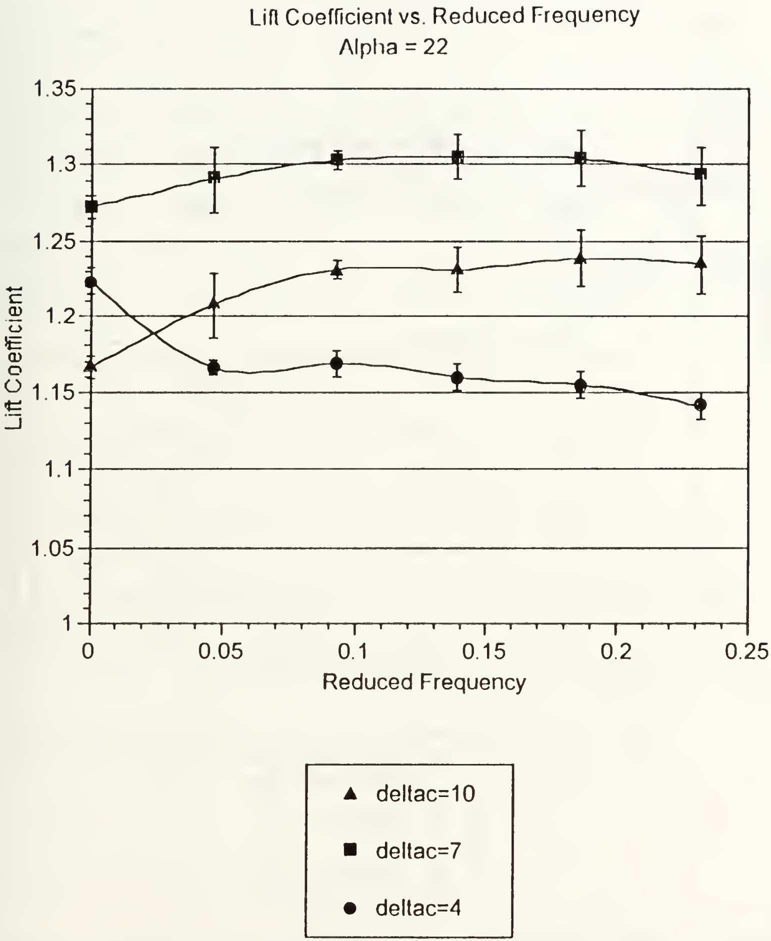

Figure 5. Alpha = 22, Deltac = +4, +7, +10

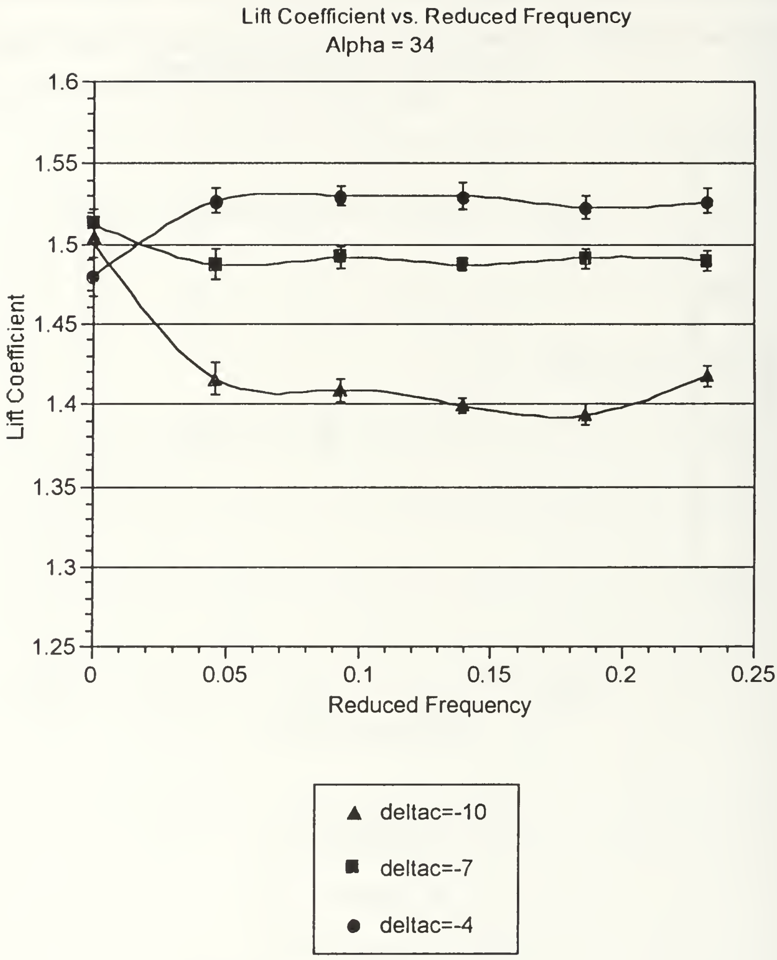

Figure 6. Alpha = 34, Deltac = -4, -7, -10

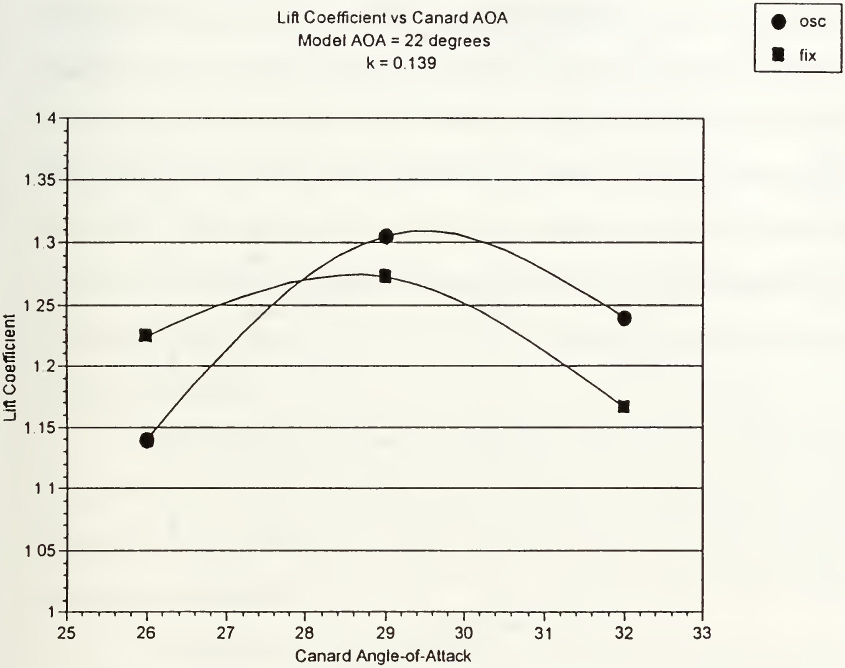

Figure 7. Summary, Alpha = 22

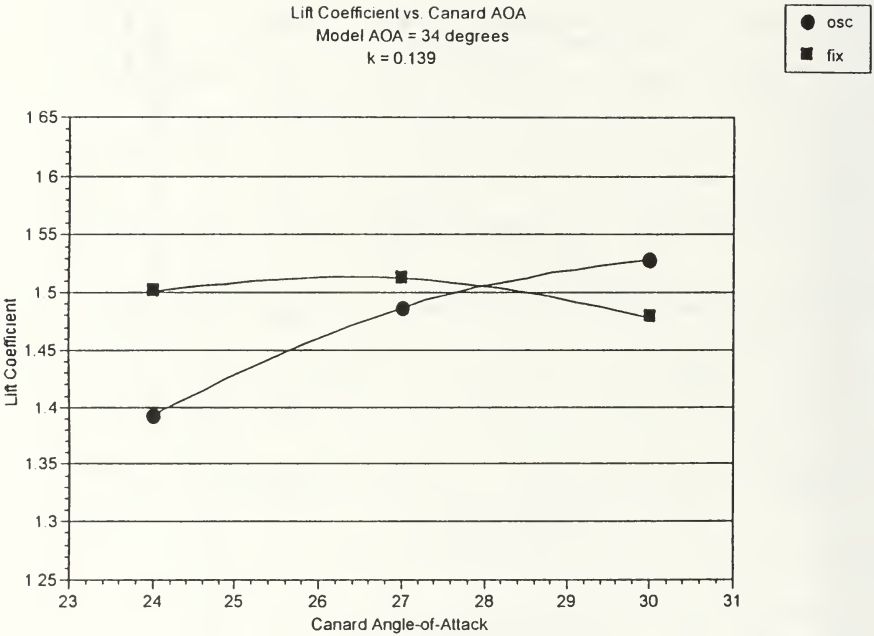

Figure 8. Summary, Alpha = 34

VI. CONCLUSIONS

Dynamic stall of a close-coupled canard was used to determine the effect on the canard/wing vortex interaction for increased lift enhancement. Two angles of attack of the model were studied: one at the first stall condition of the wing and one in the post-stall regime where a strong leading-edge vortex was formed. Mean canard deflections based on those determined to be optimum for the static case were used, as were mean values ± 3 degrees about the optimum. The amplitude of oscillation considered was ± 5 degrees about each mean; reduced frequencies tested were from 0.046 to 0.232. The following conclusions were made from the test.

- For most cases, lift was enhanced beyond the static-canard case at mean deflections equal to those at or greater than the static optimum value. The effective lift was decreased for mean deflections less than those previously determined to be optimum.

- Lift enhancements were generally 2 to 6 percent higher than the values determined with the static canard. The increased lift was generally independent of reduced frequency and peaked between k values of 0.1 to 0.2.

VII. RECOMMENDATIONS

The successes and failures encountered during this exercise result in several recommendations for further work and study. First, the strain-gage balance apparatus is in dire need of replacement. The entire cylinder should be replaced. The repair work completed was a temporary fix at best. The balance's flexure links have buckled due to overloading and misuse and its sensitivity has been reduced significantly. The rest of the strain-gage bridges will become suspect as the tunnel is continually utilized.

The oscillating mechanism within the model canard section needs several design fixes. As it now works, the arm which moves the canard is connected to the motor's shaft by set screws. These screws came loose on several test runs. An improved design would have an enlarged circular cylinder rigidly mounted to the shaft with a shear pin. The cylinder should have small indentations on its outer rim to facilitate the alteration of mean canard deflection angle. Pointed set screws which fit into these indentations would provide a more secure fitting.

The shear pin mounted on the pivot shaft of the canard failed during testing. The shaft was quickly repaired but two problems remain. The pin was replaced with a sturdier screw; however, the canard remained loose. Secondly, there is now a quarter-inch gap between the canard root chord and the model's fuselage. A larger pin will be necessary to alleviate the looseness but care must be taken to provide a streamlined canard surface. The shaft may need replacing altogether if the gap cannot be reduced.

In the study of dynamic stall of the oscillating canard, two areas require further study. Amplitude effects were not observed due to material failures. Increasing the amplitude of the oscillations may have the same effect as increasing the frequency. [Ref. 5] This remains to be verified for the three-dimensional case. Further, the range of mean canard deflections should be extended in the post-static-stall regime for these configurations and for other model angles of attack. This would quantify the effects of the model's angle of angle and the maximum lift achievable.

In designing the model, Kersh selected the 40-percent exposed root chord of the canard for the pivot point based upon Lacey's work. [Ref. 17] This position was physically located at 7-percent of the mean aerodynamic chord. No direction is given for the placement of a pivot point on a three-dimensional wing. Most two-dimensional studies [Ref. 5 & 20] utilized the airfoil quarter-chord position for oscillation. This is very near the aerodynamic center of the airfoil and thus, minimizes aerodynamic pitching-moment changes. It is recommended that the pivot point be moved to the 25-percent mean aerodynamic chord to reduce the loading on the canard and enable a broader range of wind tunnel velocities for testing.

Finally, flow visualization could be used to yield a better understanding of the dynamic-stall phenomenon. The introduction of buoyant particles into the flowfield along with the use of high-speed photography would enable particle tracing methods to be conducted. Surface flow visualization using oil could be used to qualitatively view the changes for the oscillating and static-canard cases for the flow along the wing's upper surface.

REFERENCES

1. McAtee, Thomas P., ***Agility in Demand,*** Aerospace America, Volume 26, Number 5, pp. 36-38, May 1988.

2. Skow, Andrew M., ***Agility as a Contributor to Design Balance***, Journal of Aircraft, Volume 27, Number 1, pp. 34-46, January 1992.

3. Herbst, W. B., ***Future Fighter Technologies***, Journal of Aircraft, Volume 17, Number 8, pp.561-566, August 1980.

4. Anderson, John D., ***Fundamentals of Aerodynamics***, McGraw-Hill, Inc., 1984.

5. Carr, Lawrence W., ***Progress in Analysis and Prediction of Dynamic Stall***, AIAA Journal, Volume 25, Number 1, pp.6-17, January 1988.

6. Hummel, Dietrich, and Oelker, Hans-Christoph, ***Investigations on the Vorticity Sheets of a Close-Coupled Delta-Canard Configuration***, Journal of Aircraft, Volume 26, Number 7, pp. 657-666, July 1889.

7. Er-El, J., ***Effect of Wing/Canard Interference on the Loading of a Delta Wing***, Journal of Aircraft, Volume 25, Number 1, pp.18-24, January 1988.

8. Mouch, T., McLaughlin, T., and Ashworth, J., ***Unsteady Flows Produced by Small Amplitude Oscillations of an X-29 Model***, AIAA Paper 89-2229, 1989.

9. Ashworth, J., Mouch, T., and Luttges, M., ***Visualization and Anemometry Analyses of Forced Unsteady Flows about an X-29 Model,*** AIAA Paper 88-2570, 1988.

10. Ashworth, J., Crisler, W., and Luttges, M., ***Vortex Flows created by Sinusoidal Oscillation of Three-Dimensional Wings***, AIAA Paper 89-2227, 1989.

11. Kersh, John M., Jr., ***Lift Enhancement using Close-Coupled Canard/Wing Vortex Interaction,*** Master's Degree Thesis, U.S. Naval Postgraduate School, Monterey, CA, December 1990.

12. ***Laboratory Manual for Low-Speed Wind Tunnel Testing***, Department of Aeronautics and Astronautics, Naval Postgraduate School, Monterey, CA, August 1989.

13. Holman, J. P., and Gajda, W. J., Jr., ***Experimental Methods for Engineers, 5th Ed.***, McGraw-Hill Publishing C., 1989.

14. Rae, William H., and Pope, Alan, ***Low-Speed Wind Tunnel Testing***, John Wiley and Sons, Inc., 1984.

15. Pope, Alan, and Harper, John J., ***Low-Speed Wind Tunnel Testing***, John Wiley and Sons, Inc., 1966.

16. Behrbom, H., ***Basic Low Speed Aerodynamics of the Short Coupled Canard Configuration of Small Aspect Ratio***, SAAB Aircraft Co., Rept. SAAB TN-60, July 1965.

17. Lacey, David W., ***Aerodynamic Characteristics of the Close-Coupled Canard as Applied to Low-to-Moderate Swept Wings, Volume 1: General Trends***, DTNSRDC-79/001, January 1979.

18. Schefter, Jim, ***X-31 How They're Inventing a Radical Way to Fly***, Popular Science, pp. 58-64, February 1989.

19. ***MC-MIO-16 User Manual***, National Instruments Corp., January 1989.

20. Chandrasekhara, M.S., and Brydges, B.E., ***Amplitude Effects on Dynamic Stall of an oscillating Airfoil***, AIAA Paper 90-0575, January 1990.

21. Gallaway, C.R. and Osborn, R.F., ***Aerodynamics Perspective of Supermaneuverability***, AIAA Paper 85-4068, October 1985.

22. Raymer, Daniel P., ***Aircraft Design: A Conceptual Approach***, AIAA, Inc., 1989.

APPENDIX A: MODEL DESIGN

The design parameters of the canard/wing model were established by Kersh in his study of close-coupled canard/wing vortex interaction. Aspect ratios of 2 for the canard and 3 for the wing were used, based upon the earlier work of Behrbohm. [Ref. 16] A leading-edge sweep of 60 degrees for the canard and 50 degrees for the main wing were selected to ensure strong leading edge vortices for lift enhancement. The canard and wing were straight-tapered and taper ratios of 0.1 and 0.15 respectively were chosen based upon existing aircraft designs. Equations (A1), (A2), and (A3) were used to derive the planform dimensions. [Ref. 22]

$$AR=2\frac{b}{C_r(1+\lambda)} \tag{A1}$$

$$AR=\frac{b^2}{S} \tag{A2}$$

$$MAC=\frac{2}{3}\left(C_r+C_t-\frac{C_rC_t}{C_r+C_t}\right) \tag{A3}$$

Where:

AR	- Aspect Ratio
b	- Wing span
C_r	- Length of root chord
C_t	- Length of tip chord
λ	- Taper ratio C_t/C_r
S	- Area of wing
MAC	- Wing mean aerodynamic chord

The NACA 64A008 airfoil section was chosen for both the wing and the canard based upon Lacey's previous work.[Ref. 17] A rounded leading edge for the wing and canard was used in this design to more closely model what is found on a number of existing aircraft. No attempt was made to trip the boundary layer. The Reynolds number based upon the wing mean aerodynamic chord was 7.7×10^5. Figure A1 gives the geometric characteristics of the canard and wing. The 40-percent exposed root chord of the canard and the quarter-chord of the MAC of the wing with respect to the centerline of the fuselage were the reference points used for the longitudinal separation of the canard and wing. The ratio of the longitudinal separation of the canard 40-percent exposed root chord point from the 25-percent wing mean aerodynamic chord point, relative to the wing mean aerodynamic chord, x/MAC, was 1.2. This resulted in a 2.33-inch separation between the exposed trailing edge of the canard and the exposed leading edge of the wing. Vertically, the canard was positioned so that the non-dimensional distance of the canard above the wing, z/MAC, equaled 0.2. This resulted in a 1.9-inch vertical separation between the canard and wing planes. The pivot point of the canard was 40 percent of the exposed root chord. The pivot point of the balance was 17.18 inches from the tip of the model. The model's length of 36 inches, width of 4.5 inches, height of 3 inches, and semi-span, measured from the reflection plane to the wing tip, of 12.1 inches ensured that the balance would be loaded by large forces while the tunnel was in operation. Figure A2 depicts the wing/canard/body model. Although the model was initially tested with a fixed canard, adequate space for a canard positioning motor was included in the design. A rotary-arm mechanism with electric motor was then designed and built by lab personnel to positively control the canard at all tunnel ΔP's. The electric cabling for the model was led through a hole in the model tail to a controller outside of the tunnel. The canard was oscillated using the controller and a variable DC power supply. Lines drawn on the body at the trailing edge of the canard depicted degrees of canard deflection from the body centerline. Figures A3 and A4 show the model and canard positioning motor. [Ref. 11]

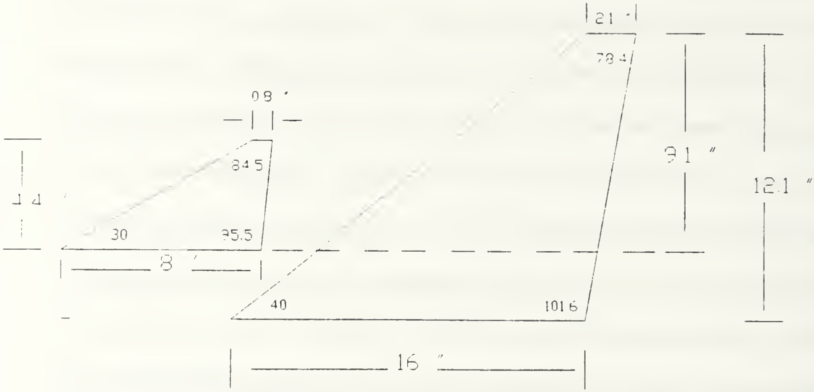

Figure A1. Canard and Wing Sketch

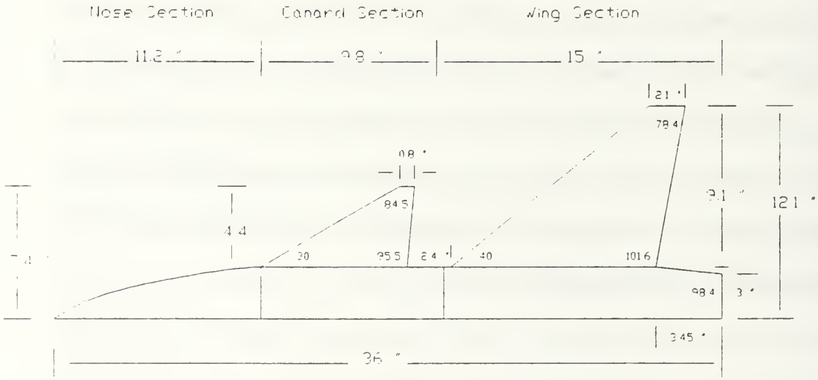

Figue A2. Canard/Wing Model Sketch

Figure A3. Canard/Wing Model

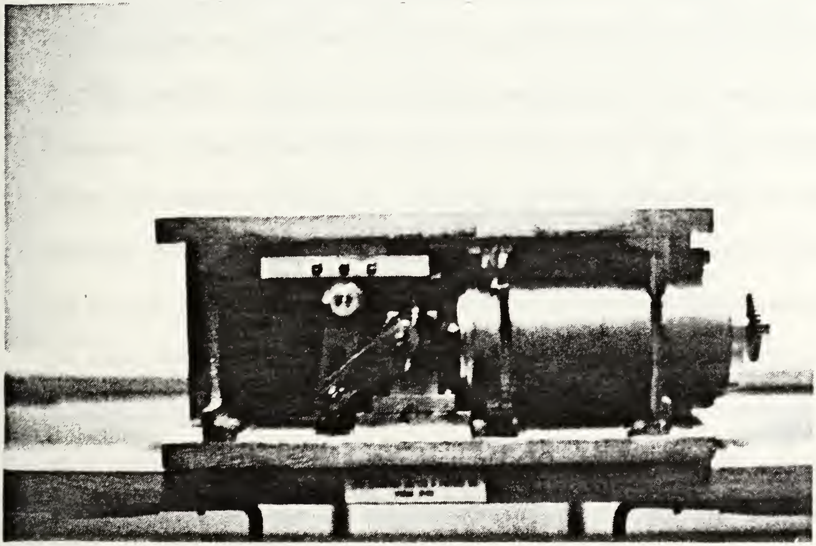

Figure A4. Canard Positioning Motor

APPENDIX B: BALANCE CALIBRATION

The externally-mounted cylindrical strain-gage balance used was built to measure axial and normal forces and pitching moment in the NPS low-speed wind tunnel. Each external strain-gage bridge had four active legs for automatic temperature compensation. The normal and axial moments were measured by two orthogonal strain-gage bridges cemented to the flexure links on the balance column at positions A and B separated by a vertical distance of 26.5 inches, as shown in Figure B1. With the wind tunnel in operation, the forces on the model created a different moment on the upper, bridge B, and the lower, bridge A, strain-gage bridges. With the operational amplifiers set to a gain of 1000 and the 12-bit MC-MIO-16-9 board set for a gain of 1, the system was capable of analog-to-digital conversion with a 4.88-mvolt resolution. An R.M.S. voltmeter was used to verify that electrical noise in the system was less than 1.5 mvolts. The calibration procedure consisted of rotating the balance turntable to either 0 or 90 degrees and suspending weights from the rig at two different heights. A horizontal beam with a pulley mechanism was designed by NPS laboratory personnel to support the calibration weights. The beam was bolted horizontally to the side opening of the wind tunnel test section. The pulley was mounted vertically at the center of the

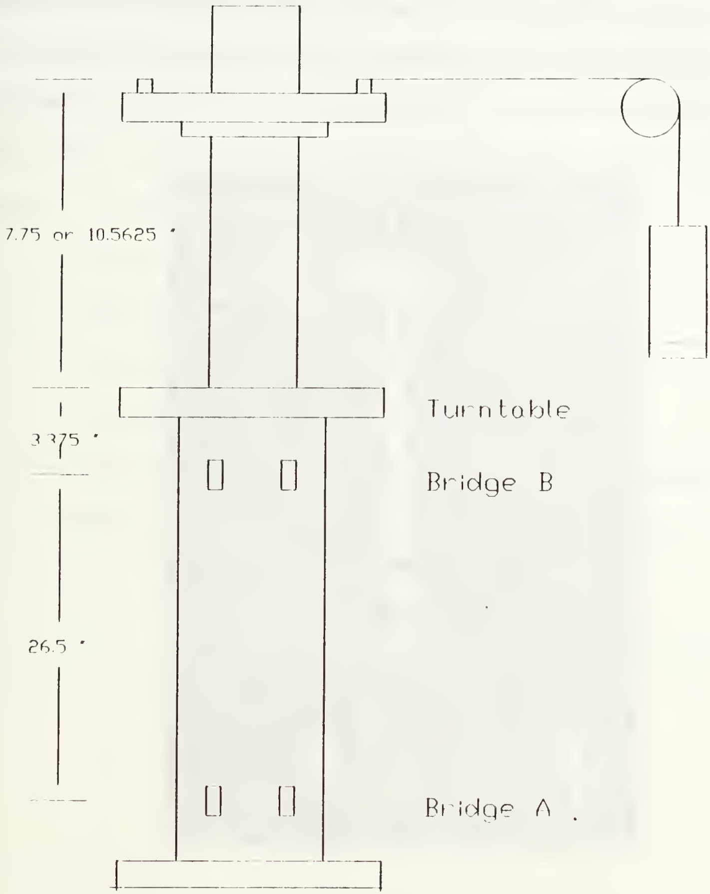

Figure B1. Strain-gage Balance Diagram

beam. Its height was adjustable so that the cable could remain horizontal. Figure B2 shows a photograph of the balance used to measure the forces and the rotating turntable used to position the model at various angles of attack.

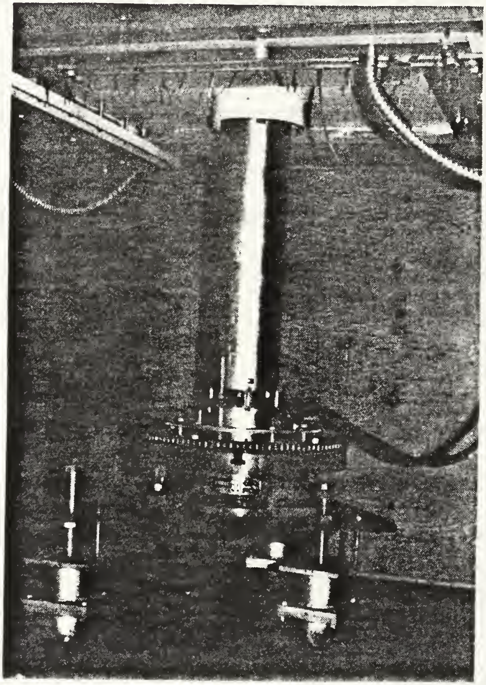

Figure B2. Balance and Turntable

Figure B3 shows the wiring diagram of the strain-gage bridges. Axial forces were measured parallel to the tunnel walls. Normal forces were perpendicular to the walls. Figure B4 illustrates the sign convention used. Note that the balance was rotated 90 degrees when the wing/canard/body model was mounted. This was to account for the turntable rotational limits of -18 to +200 degrees of revolution. Balance nomenclature is as follows:

Ean	-Voltage at the lower normal force bridge
Eaa	-Voltage at the lower axial force bridge
Ebn	-Voltage at the upper normal force bridge
Eba	-Voltage at the upper axial force bridge
(a - b)	-Height above turntable of first cable attachment point (10.5625 in.)
(a' - b)	-Height above turntable of second cable attachment (7.75 in.)

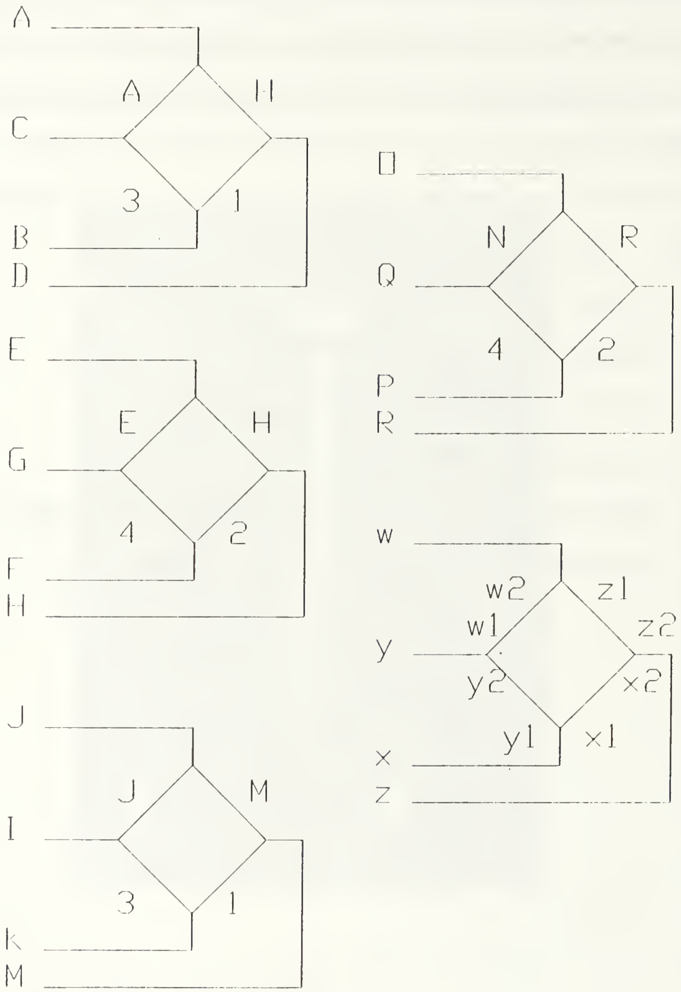

Figure B3. Strain-gage Wiring Diagram

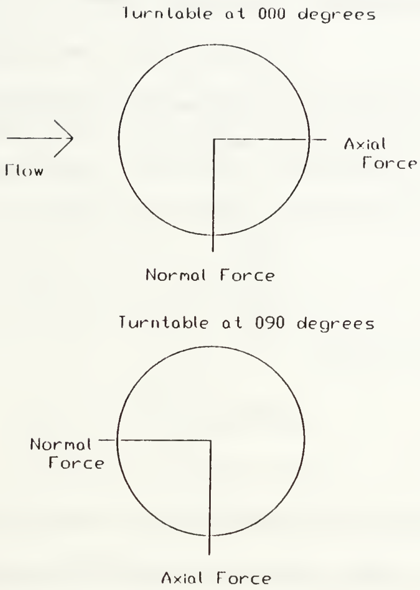

Figure B4. Sign Convention

Equation (B1) was the basic equation used in determining the axial and normal forces and moments.

$$[K]\left[\frac{d\Delta E}{dLOAD}\right]=\begin{bmatrix}\frac{FORCES}{FORCES} & 0\\ \frac{FORCES}{MOMENTS} & 0\\ 0 & \frac{FORCES}{FORCES}\\ 0 & \frac{FORCES}{MOMENTS}\end{bmatrix} \qquad \text{(B1)}$$

Expanding equation (B1) into 4 X 4 matrices yields:

$$\begin{bmatrix} K_{11} & K_{12} & K_{13} & K_{14} \\ K_{21} & K_{22} & K_{23} & K_{24} \\ K_{31} & K_{32} & K_{33} & K_{34} \\ K_{41} & K_{42} & K_{43} & K_{44} \end{bmatrix} \begin{bmatrix} d\Delta Eaa/dA & d\Delta E'aa/dA & d\Delta Eaa/dN & d\Delta E'aa/dN \\ d\Delta Eba/dA & d\Delta E'ba/dA & d\Delta Eba/dN & d\Delta E'ba/dN \\ d\Delta Ean/dA & d\Delta E'an/dA & d\Delta Ean/dN & d\Delta E'an/dN \\ d\Delta Ebn/dA & d\Delta E'bn/dA & d\Delta Ebn/dN & d\Delta E'bn/dN \end{bmatrix} =$$

$$\begin{bmatrix} 1 & 1 & 0 & 0 \\ (a-b) & (a'-b) & 0 & 0 \\ 0 & 0 & 1 & 1 \\ 0 & 0 & (a-b) & (a'-b) \end{bmatrix} \qquad \text{(B2)}$$

The right hand side of equation (B2) was known. The calibration process served to determine the voltage slopes as the balance was loaded and the [K] matrix was found by inverting the dΔE/dLoad matrix. Prior to loading the rig, the operational amplifier inputs and outputs were zeroed. The span voltages were then set to 10 volts and the signal zeroes were adjusted to 0 ± 0.05 volts. Weights measured to three-digit accuracy were then suspended from the rig and increased in increments of 5 and 10 lbf. in the normal and axial directions. Two different values for the height of the cable, (a - b) = 10.5625 in. and (a' - b) = 7.75 in., were used to resolve the moments. Corresponding voltages at each strain-gage were recorded and assembled in data files. The slopes of the voltage variations were determined using the linear regression function of Microsoft Excel®.

To illustrate; dΔEaa/dA represents the slope of the voltage Eaa versus weight as the rig is loaded axially at the 10.5625-inch height.

The normal and axial forces and moments on the model could then be found using equation (B3).

$$\begin{bmatrix} A \\ n \\ N \\ l \end{bmatrix} = \begin{bmatrix} 1 & 0 & 0 & 0 \\ 0 & 1 & 0 & 0 \\ 0 & 0 & 1 & 0 \\ 0 & 0 & 0 & 1 \end{bmatrix} [K] \begin{bmatrix} Eaa \\ Eba \\ Ean \\ Ebn \end{bmatrix} \tag{B3}$$

Where: A,N - Axial and Normal Forces (lbf)

n,l - Yaw and Roll Moments (ft lbf)

The non-dimensional coefficients, C_N and C_A, were found using equations similar to (4) and (5). C_L and C_D were found using equations (B4) and (B5).

$$C_L = C_N * \cos(\alpha) - C_A * \sin(\alpha) \tag{B4}$$

$$C_D = C_N * \sin(\alpha) + C_A * \cos(\alpha) \tag{B5}$$

Figures B9 through B12 graphically depict the voltage variations as the calibration rig was loaded in both the axial and normal directions. The calibration data is enclosed in Tables B1 through B4. Linear regression summaries along with error analyses are included at the bottom of each table.

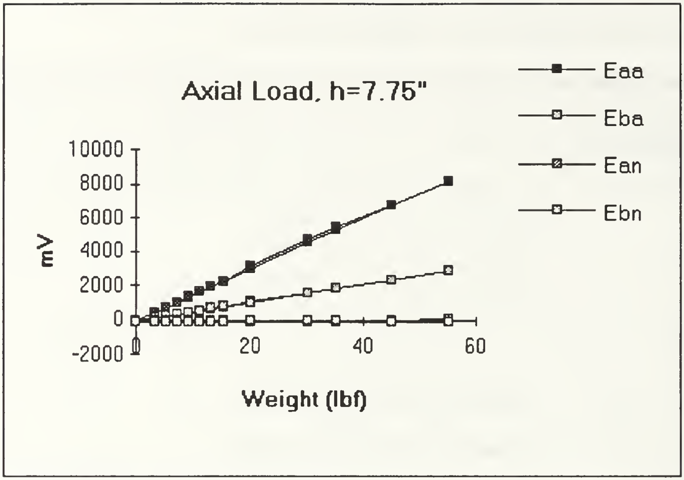

Figure B9: Calibration loading

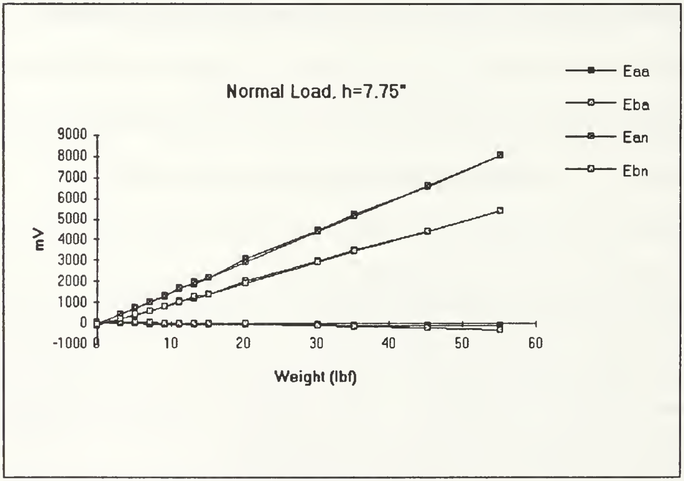

Figure B10: Calibration Loading

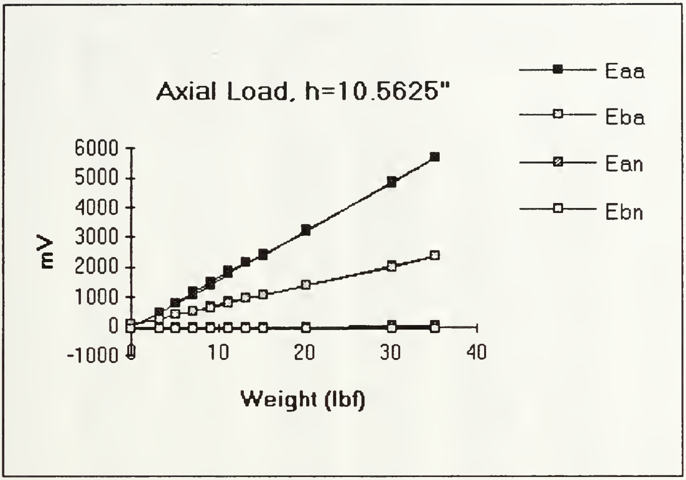

Figure B11: Calibration Loading

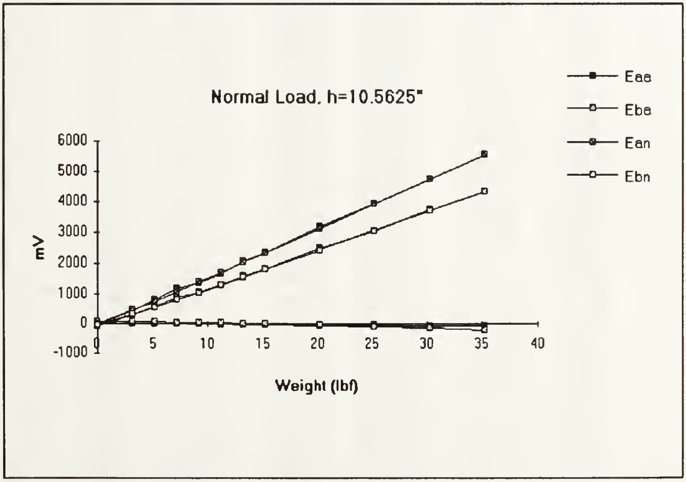

Figure B12: Calibration Loading

TABLE B1: AXIAL LOADING, H=7.75"

Axial Load		h=7.75"					
Weight	Eaa	Eba	Ean	Ebn			
0	-0.02441	-3.33008	-30.0732	-65.3564			
0	-0.0293	-3.21777	-29.9316	-65.4688			
0	-0.01953	-3.03711	-30.083	-65.5518			
0	-0.00488	-3.14453	-29.9658	-64.9512			
3.204	476.1914	158.423	-24.4775	-63.4521			
3.204	475.4248	157.998	-24.5703	-63.7842			
3.204	475.1807	157.954	-24.4775	-63.6719			
3.204	474.2969	157.744	-24.4482	-64.0918			
5.2	717.7783	241.646	-24.3066	-62.9883			
5.2	716.8311	240.928	-24.3604	-63.0957			
5.2	715.752	240.767	-24.3359	-63.0811			
5.2	715.3271	240.205	-24.2627	-63.2373			
7.207	1007.881	339.995	-19.5166	-62.8613			
7.207	1006.968	339.522	-19.5166	-62.9541			
7.207	1005.361	339.165	-19.5117	-62.9639			
7.207	1004.805	339.102	-19.5117	-63.0518			
9.21	1319.497	444.805	-15.6738	-62.7441			
9.21	1318.32	444.004	-16.9482	-62.5781			
9.21	1317.212	443.804	-16.1279	-62.1924			
9.21	1316.177	443.706	-15.542	-62.4756			
9.21	1315.742	443.325	-15.0195	-62.4414			
11.214	1684.038	565.776	-13.4863	-61.2354			
11.214	1683.921	565.405	-13.2861	-60.9277			
11.214	1683.452	565.435	-13.3936	-61.5137			
11.214	1682.954	565.103	-13.1836	-62.0898			
13.219	1936.948	654.502	-9.75586	-61.4795			
13.219	1935.352	653.696	-9.76074	-61.3623			
13.219	1933.779	653.267	-9.75586	-61.6504			
13.219	1932.935	652.822	-9.75586	-61.9727			
15.223	2257.744	766.875	-7.86133	-60.7568			
15.223	2256.147	766.494	-7.55859	-61.0986			
15.223	2254.849	765.718	-7.05566	-60.8838			
15.223	2253.955	765.996	-6.35742	-60.9619			
20.233	3125.903	1071.95	0.498047	-59.4629			
20.233	3124.395	1070.74	0.527344	-59.3408			
20.233	3122.754	1070.74	0.493164	-58.9063			
20.233	3120.894	1069.97	0.678711	-58.6963			
30.236	4691.333	1607.08	14.31641	-58.0615			
30.236	4688.755	1606.11	14.25293	-58.2813			
30.236	4686.528	1605.02	14.27246	-58.2715			
30.236	4684.966	1604.61	14.21387	-58.5205			
35.242	5447.676	1869.58	19.28711	-58.2617			

35.242	5442.495	1867.72	19.5459	-58.1836			
45.244	6741.177	2316.51	28.70606	-58.2715			
45.244	6736.66	2315.27	28.76953	-58.2422			
45.244	6733.574	2314.44	28.7207	-58.0566			
45.244	6729.819	2312.88	28.75977	-57.959			
55.248	8191.704	2825.47	37.12891	-60.2979			
55.248	8182.231	2822.47	37.03613	-60.3906			
55.248	8177.139	2821.01	36.85547	-60.7178			
55.248	8174.16	2820.3	36.97754	-60.6104			
45.244	6738.53	2328.48	30.21973	-56.5576			
45.244	6736.006	2327.62	30.1709	-56.8213			
45.244	6733.516	2326.89	30.20996	-56.2256			
45.244	6731.792	2325.83	30.24902	-57.1924			
35.242	5253.608	1830.83	21.12793	-54.917			
35.242	5252.813	1830.3	20.28809	-54.7559			
35.242	5249.463	1829.15	20.27832	-54.7949			
35.242	5247.573	1828.66	20.22949	-55.4639			
30.236	4520.259	1576.64	15.3125	-54.7314			
30.236	4519.741	1576.31	15.19043	-54.3457			
30.236	4519.199	1576.72	15.15137	-54.0186			
30.236	4518.662	1576.3	15.30273	-54.3457			
20.233	2989.595	1053.71	1.010742	-56.665			
20.233	2988.486	1053.72	0.722656	-57.0605			
20.233	2987.896	1053.03	0.795898	-57.0459			
20.233	2987.422	1052.87	1.230469	-56.6895			
15.223	2262.227	800.181	-4.94629	-58.0518			
15.223	2261.729	799.722	-4.96582	-58.0811			
15.223	2261.563	799.634	-4.94629	-57.4023			
15.223	2261.699	799.443	-4.94629	-57.2461			
15.223	2261.309	799.78	-4.90234	-57.3193			
13.219	1947.998	690.962	-9.71191	-58.4863			
13.219	1947.583	690.947	-9.73145	-58.3447			
13.219	1947.173	690.518	-9.70703	-58.5205			
13.219	1947.134	690.542	-9.72656	-58.4131			
13.219	1946.821	690.898	-9.69727	-58.3008			
11.214	1636.221	583.189	-11.9873	-59.1602			
11.214	1636.602	582.817	-12.6416	-58.8672			
11.214	1636.719	582.93	-13.0957	-58.9648			
11.214	1636.729	583.149	-12.6074	-58.8086			
9.21	1360.371	489.219	-14.6338	-59.8828			
9.21	1360.952	489.048	-14.6338	-59.7363			
9.21	1360.767	489.116	-14.6338	-59.2236			
9.21	1359.243	488.926	-14.6338	-59.5654			
7.207	1038.735	382.324	-19.5117	-60.1758			
7.207	1038.647	382.036	-19.5117	-59.8242			
7.207	1038.208	381.88	-19.5117	-60.9717			
7.207	1038.052	381.846	-19.5117	-61.1572			
5.2	733.2656	278.96	-24.0039	-61.499			

5.2	731.6699	278.057	-24.0576	-61.123			
5.2	731.7432	277.959	-24.0723	-60.9619			
5.2	733.3789	278.711	-24.0723	-60.8936			
3.204	447.832	180.132	-24.873	-61.7432			
3.204	444.3359	179.17	-26.2061	-62.5879			
3.204	444.1064	178.677	-26.1475	-62.749			
3.204	444.1846	179.004	-25.6543	-62.2461			
3.204	443.6377	178.535	-25.1758	-62.4072			
0	0.9375	24.7266	-31.9531	-62.9688			
0	0.981445	24.6143	-32.2021	-63.2764			
0	1.142578	24.5068	-32.3486	-63.2178			
0	1.040039	24.4678	-32.1045	-63.1738			
••							
	Coefficients	Standard Error			Coefficients	Standard Error	
Eaa				Ean			
Intercept	-24.7759	9.244163		Intercept	-28.1355	0.381975	
x1	150.3653	0.401024		x1	1.307424	0.016571	
Eba				Ebn			
Intercept	0.370737	3.415721		Intercept	-62.1463	0.313433	
x1	51.67094	0.148178		x1	0.120979	0.013597	

TABLE B2: NORMAL LOADING, H=7.75"

Normal Load		h=7.75"					
Weight	Eaa	Eba	Ean	Ebn			
0	-9.887695	23.1299	-5.44922	-82.7881			
0	-9.863281	23.0225	-5.29297	-82.4805			
0	-9.907227	23.0371	-5.25391	-82.3389			
0	-9.858398	23.0127	-5.16113	-82.2314			
3.204	-19.51172	16.3867	446.8359	213.442			
3.204	-19.51172	16.3086	447.0313	212.881			
3.204	-19.51172	16.333	447.0752	213.081			
3.204	-19.51172	16.1426	447.3486	213.521			
5.2	-24.38477	12.7393	712.2363	391.465			
5.2	-24.375	12.6123	711.2842	391.299			
5.2	-24.36035	12.583	710.9863	390.918			
5.2	-24.37988	12.6416	710.7129	390.117			
5.2	-24.37988	12.5928	710.542	389.443			
7.207	-29.10156	8.45703	1001.929	582.432			
7.207	-29.16016	8.46191	1000.41	581.157			
7.207	-29.15527	8.34961	999.6338	580.747			
7.207	-29.0625	8.25195	999.0869	580.151			
9.21	-33.37402	3.76953	1292.456	781.113			
9.21	-33.39356	3.63281	1291.797	780.566			
9.21	-33.50586	3.68652	1291.714	780.005			
9.21	-33.33496	3.56445	1291.157	779.775			
9.21	-33.36914	3.51074	1290.991	779.199			
11.214	-38.95996	-2.91504	1687.554	1052.75			
11.214	-38.97949	-3.14941	1686.504	1051.83			
11.214	-38.96973	-3.25684	1685.537	1050.71			
11.214	-38.98926	-3.29102	1684.541	1050.59			
13.219	-42.80762	-6.21094	1873.511	1180.03			
13.219	-42.83203	-6.2207	1872.358	1178.9			
13.219	-42.86621	-6.31836	1871.323	1178.5			
13.219	-42.5293	-6.17676	1871.357	1178.12			
15.223	-47.68555	-11.6602	2184.409	1393.91			
15.223	-47.69531	-11.7529	2183.408	1393.46			
15.223	-47.59277	-11.9043	2182.754	1392.47			
15.223	-47.72949	-11.9043	2182.354	1391.5			
20.233	-61.18652	-30.4541	3059.663	1992.79			
20.233	-61.26953	-30.8203	3058.389	1991.84			
20.233	-61.02051	-31.25	3056.548	1990.6			
20.233	-60.99121	-31.2305	3055.288	1989.81			
20.233	-60.9668	-31.3037	3054.707	1989.43			
30.236	-80.96191	-87.9834	4468.882	2952.54			
30.236	-81.29883	-88.999	4464.873	2949.37			
30.236	-81.16211	-89.3506	4462.866	2947.69			

35.242	-92.92481	-134.644	5262.129	3492.31			
35.242	-92.80762	-134.917	5259.277	3490.47			
35.242	-93.05664	-135.015	5257.119	3489.03			
45.244	-112.4902	-222.236	6580.293	4390.35			
45.244	-112.3926	-222.715	6576.294	4387.05			
45.244	-112.3096	-223.247	6572.744	4384.69			
45.244	-112.2461	-223.335	6569.414	4382.77			
55.248	-134.1895	-335.586	8051.323	5391.52			
55.248	-134.1748	-336.353	8044.38	5385.72			
55.248	-133.9551	-336.729	8035.649	5379.47			
55.248	-133.6963	-336.782	8031.606	5376.33			
55.248	-133.8916	-336.807	8028.687	5374			
45.244	-109.7705	-230.244	6613.623	4411.33			
45.244	-109.8682	-230.439	6611.909	4409.58			
45.244	-109.7412	-230.459	6611.655	4409.5			
45.244	-109.7803	-230.698	6612.168	4410.24			
35.242	-88.19336	-146.572	5157.119	3418.93			
35.242	-88.20313	-146.782	5156.885	3418.54			
35.242	-88.11035	-146.528	5156.88	3417.92			
35.242	-88.30078	-146.577	5155.439	3416.88			
30.236	-77.68066	-100.928	4419.492	2915.8			
30.236	-77.77344	-101.187	4419.038	2914.84			
30.236	-77.77832	-101.099	4418.73	2914.07			
30.236	-77.61231	-101.25	4418.755	2914.04			
20.233	-55.88379	-24.7852	2934.404	1906.03			
20.233	-55.9668	-24.9219	2933.999	1905.46			
20.233	-55.81543	-25.166	2933.823	1904.87			
20.233	-55.93262	-25.0537	2933.55	1904.59			
20.233	-55.96191	-24.9365	2933.618	1904.51			
15.223	-44.58496	-6.18164	2194.624	1399.08			
15.223	-44.58496	-6.29395	2194.258	1397.9			
15.223	-44.61426	-6.04492	2194.868	1398.75			
15.223	-44.75098	-5.96191	2194.175	1398.23			
15.223	-44.7168	-6.10352	2194.272	1398.13			
13.219	-41.99707	-0.04883	1970.278	1246.15			
13.219	-42.05078	-0.13184	1971.064	1246.45			
13.219	-42.00684	-0.13672	1971.641	1247.19			
13.219	-41.97266	-0.15137	1971.982	1246.8			
11.214	-37.19238	12.9004	1617.314	1003.29			
11.214	-37.22168	12.9053	1617.173	1003.3			
11.214	-37.24121	12.959	1616.646	1002.82			
11.214	-36.96289	12.7881	1617.207	1003.16			
11.214	-36.86035	12.7832	1616.748	1002.18			
9.21	-32.76856	22.1484	1318.184	799.189			
9.21	-32.89063	21.9238	1318.296	798.94			
9.21	-33.04688	21.9531	1318.301	799.111			
9.21	-32.92481	21.9189	1317.813	799.102			
7.207	-29.12109	31.2598	1028.291	601.938			

7.207	-29.10156	31.3379	1027.817	601.934			
7.207	-29.08691	31.1768	1027.715	601.035			
7.207	-29.10156	31.3232	1027.432	601.25			
5.2	-24.37012	40.9033	726.3965	401.743			
5.2	-24.37988	41.1084	726.3525	401.758			
5.2	-24.375	41.0498	726.5088	401.963			
5.2	-24.375	41.0645	726.4111	402.529			
3.204	-19.51172	50.2783	437.9785	208.779			
3.204	-19.50684	50.1855	437.5635	209.111			
3.204	-19.5166	50.1807	437.8906	207.656			
3.204	-19.5166	50.2148	437.8467	207.168			
0	-13.36914	62.9492	-1.875	-76.9141			
0	-13.4375	63.0078	-2.04102	-76.0254			
0	-13.30566	62.9102	-1.78223	-76.4502			
0	-13.50098	62.8906	-1.8457	-75.6152			
	Coefficients	Standard Error			Coefficients	Standard Error	
Eaa				Ean			
Intercept	-12.944276	0.230756		Intercept	-20.499395	6.552537	
x1	-2.193082	0.009819		x1	146.805075	0.278807	
Eba				Ebn			
Intercept	71.654185	3.483731		Intercept	-106.57796	4.745903	
x1	-6.391158	0.148231		x1	99.945325	0.201936	

TABLE B3: AXIAL LOADING, H=10.5625"

Axial Load		h=10.5625"					
Weight	Eaa	Eba	Ean	Ebn			
0	-0.07813	86.5186	-29.2725	-67.5146			
0	-0.0293	86.3916	-29.2627	-67.5488			
0	-0.01465	86.4746	-29.2578	-67.6514			
0	-0.04883	86.4209	-29.2627	-67.832			
3.204	492.4072	291.836	-22.6953	-63.1396			
3.204	492.7393	291.841	-23.4424	-63.75			
3.204	493.042	291.704	-22.9248	-63.4668			
3.204	493.2471	291.953	-22.4365	-63.4863			
5.2	810.7666	418.897	-18.8525	-62.2656			
5.2	810.2246	418.398	-19.292	-61.8701			
5.2	809.4189	418.106	-19.2139	-61.7676			
5.2	808.9063	417.817	-18.916	-61.8896			
7.207	1164.453	558.008	-12.2021	-59.541			
7.207	1163.56	557.139	-12.876	-59.9414			
7.207	1162.734	556.523	-12.5391	-59.6484			
7.207	1162.095	556.577	-11.7383	-58.9502			
9.21	1531.597	705.273	-7.10938	-57.627			
9.21	1530.981	705.19	-7.24121	-57.6025			
9.21	1530.142	704.727	-7.02637	-57.7051			
9.21	1529.707	704.487	-7.11914	-57.5684			
9.21	1529.043	704.028	-6.63574	-57.4121			
11.214	1903.477	855.85	-0.72754	-54.1943			
11.214	1903.032	855.332	-0.93262	-53.9746			
11.214	1902.632	854.858	-0.85938	-54.0771			
11.214	1902.129	854.697	-0.73731	-54.4922			
13.219	2154.517	957.944	0.541992	-53.1934			
13.219	2152.964	957.642	0.395508	-53.1104			
13.219	2151.558	957.114	0.527344	-53.2715			
13.219	2151.089	957.344	0.825195	-53.418			
15.223	2415.957	1065.36	4.760742	-52.583			
15.223	2415.273	1064.95	4.697266	-52.5146			
15.223	2414.473	1064.28	4.6875	-51.8945			
15.223	2413.462	1063.92	4.780273	-51.6455			
20.233	3204.951	1385.51	14.54102	-48.2275			
20.233	3201.807	1384.71	14.54102	-48.3154			
20.233	3200.02	1383.73	14.58008	-48.4961			
20.233	3199.512	1383.46	14.64356	-48.4277			
20.233	3198.984	1383.14	14.70703	-48.54			
30.236	4852.729	2037.64	33.78418	-41.3965			
30.236	4849.116	2036.02	33.73535	-42.4316			
30.236	4846.831	2035.13	33.7793	-42.6367			

35.242	5684.717	2363.11	43.08106	-39.5166			
35.242	5682.041	2362.3	42.97363	-39.5801			
35.242	5678.594	2360.63	43.02734	-39.3359			
35.242	5677.29	2360.36	43.16895	-39.5264			
30.236	4836.128	2024.18	31.71875	-43.6719			
30.236	4834.648	2023.92	31.58691	-43.5107			
30.236	4833.682	2023.13	31.72852	-43.3252			
30.236	4832.661	2022.67	31.76758	-43.3594			
20.233	3241.875	1401.53	14.32617	-48.1738			
20.233	3241.191	1401.24	14.41895	-48.0029			
20.233	3240.63	1401.06	14.45801	-47.8906			
20.233	3240.815	1400.97	14.45801	-47.8369			
20.233	3240.449	1400.69	14.37988	-47.9395			
15.223	2403.325	1061.02	4.526367	-52.2754			
15.223	2403.325	1060.92	4.550781	-52.3096			
15.223	2402.822	1060.89	4.614258	-52.4316			
15.223	2402.451	1061.21	4.619141	-52.4951			
15.223	2402.559	1060.9	4.604492	-51.9971			
13.219	2153.34	958.569	0.170898	-52.8857			
13.219	2152.559	958.418	0.151367	-53.1494			
13.219	2152.139	958.145	0.161133	-53.1787			
13.219	2151.636	958.56	0.170898	-53.3838			
11.214	1781.68	808.779	-4.86328	-55.2197			
11.214	1781.797	808.198	-4.83887	-55.4492			
11.214	1781.372	808.232	-4.86816	-55.1465			
11.214	1781.387	807.881	-4.84863	-55.2441			
9.21	1417.783	660.776	-9.76074	-58.0664			
9.21	1417.612	660.786	-9.75586	-58.1006			
9.21	1417.598	661.035	-9.76074	-57.8076			
9.21	1417.222	660.923	-9.75586	-57.915			
9.21	1417.71	661.079	-9.75586	-57.7539			
7.207	1104.609	535.303	-14.6338	-58.6523			
7.207	1104.224	535.19	-14.6289	-59.0332			
7.207	1104.575	535.156	-14.6338	-58.9844			
7.207	1104.814	535.049	-14.6338	-59.1357			
7.207	1104.546	534.907	-14.6338	-58.9063			
5.2	789.707	412.212	-19.5117	-61.9824			
5.2	789.0137	412.261	-19.5068	-61.2646			
5.2	789.1992	411.939	-19.502	-60.8398			
5.2	788.7402	411.856	-19.5117	-60.957			
5.2	788.9209	411.89	-19.5117	-61.0938			
3.204	467.3535	284.063	-24.2969	-63.4375			
3.204	467.5195	284.082	-24.3457	-63.6035			
3.204	467.7539	283.97	-24.3506	-63.8281			
3.204	467.5244	283.96	-24.3066	-63.7402			
3.204	467.6611	284.053	-24.3262	-63.4717			
0	0.239258	89.3701	-29.502	-66.958			
0	0.249023	89.3701	-29.5166	-66.7383			

0	0.297852	89.2773	-29.4629	-66.7188			
0	0.288086	89.0283	-29.4775	-66.6553			
....							
	Coefficients	Standard Error			Coefficients	Standard Error	
Eaa				Ean			
Intercept	-16.1475	6.721237		Intercept	-28.4967	0.297724	
x1	160.9926	0.423445		x1	2.081286	0.018757	
Eba				Ebn			
Intercept	87.55774	2.567009		Intercept	-65.1267	0.224842	
x1	64.49639	0.161724		x1	0.782588	0.014165	

TABLE B4: NORMAL LOADING, H=10.5625"

Normal Load		h=10.5625"					
Weight	Eaa	Eba	Ean	Ebn			
0	3.989258	15.6396	-20.3516	-60.7324			
0	3.999023	15.7959	-20.1074	-60.8789			
0	4.013672	15.6885	-20.0537	-60.9912			
0	4.047852	15.7861	-20.4053	-60.874			
3.204	-4.838867	8.84277	449.2139	304.448			
3.204	-4.84375	8.76465	448.6865	304.058			
3.204	-4.824219	8.92578	448.584	303.252			
3.204	-4.775391	9.0332	448.2031	303.657			
5.2	-9.746094	2.12891	821.2402	595.298			
5.2	-9.755859	2.02637	820.5811	594.102			
5.2	-9.750977	1.95801	819.6973	592.852			
5.2	-9.755859	1.91406	820.0244	592.48			
7.207	-14.63867	-5.01465	1171.353	872.725			
7.207	-14.63379	-5.04395	1170.376	872.964			
7.207	-14.63379	-5.01953	1170.449	872.173			
7.207	-14.62891	-4.99512	1170.103	872.427			
9.21	-17.41699	-9.75098	1374.307	1034.95			
9.21	-17.36328	-9.76074	1372.822	1034.11			
9.21	-17.05078	-9.76563	1372.085	1032.98			
9.21	-16.98242	-9.75586	1371.602	1032.34			
11.214	-20.34668	-17.9932	1681.011	1279.93			
11.214	-20.5957	-18.2324	1679.419	1278.71			
11.214	-20.10742	-18.5986	1678.301	1277.64			
11.214	-20.17578	-18.2666	1677.588	1277.45			
13.219	-26.00098	-29.1797	2065.234	1586.89			
13.219	-26.05469	-29.1504	2063.335	1585.41			
13.219	-25.80078	-29.1797	2062.051	1583.7			
13.219	-25.80078	-29.2041	2061.504	1582.7			
15.223	-29.3457	-38.7305	2348.95	1812.68			
15.223	-29.30176	-38.75	2346.792	1809.56			
15.223	-29.32129	-38.7646	2345.41	1808.79			
15.223	-29.28711	-38.6621	2344.268	1807.29			
20.233	-41.21094	-68.1592	3180.684	2473.45			
20.233	-41.2793	-68.0713	3177.988	2472.06			
20.233	-41.17676	-67.9053	3176.665	2470.24			
20.233	-40.93262	-67.8125	3175.371	2468.45			
25.239	-51.43555	-104.067	3910.342	3048.33			
25.239	-51.40137	-103.989	3908.721	3046.62			
25.239	-51.3916	-104.048	3907.48	3045.91			
25.239	-51.31348	-103.613	3906.055	3045.21			
30.236	-62.54395	-160.654	4756.338	3719.79			

30.236	-62.41699	-160.156	4750.869	3715.83			
35.242	-72.7002	-217.705	5545.967	4345.74			
35.242	-72.47559	-217.539	5542.134	4342.15			
35.242	-72.55371	-217.363	5539.98	4340.64			
35.242	-72.55859	-217.148	5537.798	4338.61			
30.236	-63.44238	-149.243	4726.23	3696.58			
30.236	-63.26172	-149.106	4725.132	3695.79			
30.236	-63.37402	-148.984	4724.385	3694.03			
30.236	-63.51074	-149.058	4723.95	3693.08			
20.233	-41.7334	-35.835	3115.352	2423.75			
20.233	-41.8457	-35.7861	3115.063	2423.43			
20.233	-41.66504	-36.0449	3114.966	2423.02			
20.233	-41.7334	-35.9326	3114.673	2422.66			
15.223	-29.39941	0.35156	2331.982	1800.67			
15.223	-29.38477	0.42481	2331.67	1800.88			
15.223	-29.29688	0.34668	2331.753	1800.75			
15.223	-29.33106	0.37598	2331.514	1800.19			
15.223	-29.32617	0.41992	2331.108	1800.43			
13.219	-25.3418	12.6709	2026.416	1558.69			
13.219	-25.27344	12.6367	2025.869	1558.02			
13.219	-25.1709	12.5146	2025.884	1557.72			
13.219	-25.23926	12.6172	2025.742	1557.58			
11.214	-22.26563	24.0039	1708.247	1304.63			
11.214	-21.95801	23.8281	1708.125	1304.39			
11.214	-22.12891	23.999	1708.237	1304.16			
11.214	-22.59766	23.9844	1708.081	1303.62			
11.214	-22.37305	24.0479	1707.988	1304.06			
9.21	-18.22266	34.8828	1390.962	1052.37			
9.21	-18.51074	34.7217	1390.2	1052.24			
9.21	-18.29102	34.8633	1389.932	1052.29			
9.21	-18.03711	34.8096	1390.2	1052.22			
9.21	-18.39844	34.624	1389.961	1051.39			
7.207	-13.29102	45.5078	1070.371	797.769			
7.207	-12.97363	45.2734	1070.215	797.666			
7.207	-12.81738	45.4639	1069.868	797.334			
7.207	-13.35449	45.5469	1069.663	796.685			
7.207	-13.31055	45.5811	1069.478	797.026			
5.2	-9.370117	55.5615	742.8223	537.91			
5.2	-9.345703	55.5127	742.4316	537.144			
	Coefficients	Standard Error			Coefficients	Standard Error	
Eaa				Ean			
Intercept	2.564045	0.161644		Intercept	-45.7403	5.413727	
x1	-2.15315	0.009956		x1	157.7453	0.333457	
Eba				Ebn			
Intercept	72.54808	4.799721		Intercept	-85.4048	4.320142	
x1	-7.1007	0.295637		x1	124.9899	0.266098	

APPENDIX C: EXPERIMENTAL CORRECTIONS

Wind tunnel boundary corrections to the dynamic pressure and velocity were made for "solid blockage" only. Solid blockage affects the flowfield velocity through the test section. It is a function of model thickness and size. The model's cross-sectional area effectively reduces the area in the test section through the flow must pass. [Refs 14 & 15] The equations used were :

$$q = q_m (1 + 2*\varepsilon)$$

$$U = U (1+ \varepsilon)$$

$$\varepsilon = (\text{Model cross-section/Tunnel cross-section})*\text{SIN}(\alpha) + (\text{Canard cross-section/Tunnel cross-section})*\text{SIN}(\alpha + \delta_{canard})$$

Where:

q	-	Dynamic Pressure (lbf/ft^2)
q_m	-	Measured Dynamic Pressure (lbf/ft^2)
U	-	Velocity (ft/sec)
U_m	-	Measured Velocity (ft/sec)
ε	-	Blockage Factor
α	-	Model Angle-of-Attack
δ_{canard}	-	Canard Deflection Angle

Signal drift was measured after each tunnel run. The wind-tunnel was secured and the airspeed allowed to decay to zero. Voltage readings were taken and the corresponding zero-load lift and drag values were then subtracted from all readings taken during the run. As described in Chapter IV, the system signal drift was assumed to be a hysteresis effect of loading the strain-gage balance. All data readings were corrected for this drift.

Though wall effects may be significant for this model at high-lift conditions, absolute values for a complete trimmed aircraft configuration were not being sought. A comparison of the static-canard with the oscillating-canard effects was the desired goal. No wall corrections were made for this test.

APPENDIX D: DATA ACQUISITION CODE

```
'      This program was written and compiled using LabWindows and QuickBasic
'  4.5.  (used "bc /o multi" to compile)  Its purpose was to read and convert
' voltages from four channels connected to the strain gauges on the Academic
' wind tunnel.  The voltages are converted to normal and axial forces and moments
' with respect to the balance.  It was written and modified by LT Tom D. Stuart and
' LT Dean C. Schmidt, 20 June 92.

'  Variables explained

'       eaa = Strain gauge voltage at point A in Axial direction.
'       eba = Strain gauge voltage at point B in Axial direction.
'       ean = Strain gauge voltage at point A in Normal direction.
'       ebn = Strain gauge voltage at point B in Normal direction.

'       AX  = Axial force
'       Max = Axial moment
'       NORM = Normal force
'       Mnorm = Normal moment

'       alpha = Angle of Attack of the model
'       LIFT = Lift force
'       DRAG = Drag force

'*****************************************************************************

REM    $INCLUDE: 'C:\LW\INCLUDE\LWSYSTEM.INC'
REM    $INCLUDE: 'C:\LW\INCLUDE\GPIB.INC'
REM    $INCLUDE: 'C:\LW\INCLUDE\FORMATIO.INC'
REM    $INCLUDE: 'C:\LW\INCLUDE\GRAPHICS.INC'
REM    $INCLUDE: 'C:\LW\INCLUDE\ANALYSIS.INC'
REM    $INCLUDE: 'C:\LW\INCLUDE\DATAACQ.INC'
REM    $INCLUDE: 'C:\LW\INCLUDE\RS232.INC'

DIM K#(4,4)
DIM ean.array#(1000),eaa.array#(1000),ebn.array#(1000),eba.array#(1000)
COMMON SHARED ean.array#(),eaa.array#(),ebn.array#(),eba.array#()
```

```
DECLARE SUB volt (ean#,eaa#,ebn#,eba#,alpha#)
DECLARE SUB aero (AX#,NORM#,LIFT#,DRAG#,alpha#)
DECLARE SUB forces
(K#(),eaa#,eba#,ean#,ebn#,AX#,Max#,NORM#,Mnorm#,alpha#)

SCREEN 9, 0
COLOR 15, 1

eaa0# = 0
eaa0# = 0
ean0# = 0
ebn0# = 0

'***************************************************************************

' CALIBRATION MATRIX INPUT (See thesis for explanation)

DATA  0.009198, -0.006908,  0.000171, -0.000300
DATA -0.035913,  0.259331,  0.002494,  0.007624
DATA -0.000418,  0.000835,  0.010422, -0.005071
DATA -0.001896,  0.004440, -0.022291,  0.116806

FOR L% = 1 TO 4: FOR M% = 1 TO 4
READ K#(L%,M%) : NEXT M%
NEXT L%

'***************************************************************************

LOCATE 10, 20: INPUT "Type the name of the voltage file"; VOL$
VOL$ = "C:\LW\INSTR\" + VOL$ + ".DAT"
OPEN VOL$ FOR APPEND AS #1

CLS: LOCATE 10, 20: INPUT "Type the name of the FORCE / MOMENT file";
FM$
FM$ = "C:\LW\INSTR\" + FM$ + ".DAT"
OPEN FM$ FOR APPEND AS #2

CLS: LOCATE 10, 20: INPUT "Type the name of the Lift / Drag file"; LD$
LD$ = "C:\LW\INSTR\" + LD$ + ".DAT"
OPEN LD$ FOR APPEND AS #3
```

```
CLS: LOCATE 10, 20: INPUT "Input the Test AOA (deg.)"; alpha#

500
CLS: LOCATE 5, 20: INPUT "Is this a tare (zero load) reading? (Y/N)"; A$

IF A$ = "Y" THEN CALL tare (ean0#,eaa0#,ebn0#,eba0#,alpha#)

LOCATE 23,15: INPUT "Ready to take readings? (Y/N)"; B$

IF B$ = "Y" THEN CALL volt (ean#,eaa#,ebn#,eba#,alpha#)
IF B$ <> "Y" THEN GOTO 5000

' Correcting for zero load values.

eaa# = eaa# - eaa0#
eba# = eba# - eba0#
ean# = ean# - ean0#
ebn# = ebn# - ebn0#

CALL forces (K#(),eaa#,eba#,ean#,ebn#,AX#,Max#,NORM#,Mnorm#,alpha#)

CALL aero (AX#,NORM#,LIFT#,DRAG#,alpha#)

PRINT " "
PRINT "     AOA       EAA (mV)     EBA (mV)     EAN (mV)      EBN
(mV)"
PRINT "   **********    **********   **********   **********   **********"

PRINT USING "   ####.######";  alpha#; eaa#; eba#; ean#; ebn#
PRINT #1, USING "#####.######"; alpha#; eaa#; eba#; ean#; ebn#

PRINT " "
PRINT "   AXIAL (lb)    MOMax (ft-lb)  NORMAL (lb)   MOMnorm(ft-lb)"
PRINT "   **********    *************  ***********   ***************"

PRINT USING "   ####.######";  AX#; Max#; NORM#; Mnorm#
PRINT #2, USING "#####.######";  AX#; Max#; NORM#; Mnorm#

PRINT " "
PRINT "    Lift (lb)     Drag (lb)"
PRINT "   ***********   ***********"
```

```
PRINT USING "    ####.######"; LIFT#; DRAG#
PRINT #3, USING "#####.######"; LIFT#; DRAG#

LOCATE 23, 15: INPUT "Do you want another reading?  (Y/N)"; ANS$
IF ANS$ = "Y" THEN GOTO 500

5000 CLOSE #1
CLOSE #2
CLOSE #3

END

'**************************************************************************
'**************************************************************************
SUB volt (ean#,eaa#,ebn#,eba#,alpha#)
'**************************************************************************
'
' S/R to read Channel 0,2,4,6 on MIO-16L-9 for Analog Voltage
'
'**************************************************************************

'  Setting Board code for MIO-16L-9

board.code%=0

'**************************************************************************


err1.num% = Init.DA.Brds(1, board.code%)

err2.num% = AI.Setup(1, 0, 1)
err3.num% = AI.Setup(1, 2, 1)
err4.num% = AI.Setup(1, 4, 1)
err5.num% = AI.Setup(1, 6, 1)

' Configure and set clock to 1MHZ

err6.num% = CTR.Clock (1, 1, 1, 1)
err7.num% = CTR.Config (1, 1, 0, 0, 0, 0)

LWtotal! = 0
```

```
FOR i% = 1 TO 1000

err8.num% = CTR.EvCount (1, 1, 1, 0)

' CH 0 = Eaa
        err9.num% = AI.Read(1, 0, 1, value0%)
        er10.num% = AI.Scale(1, 1, value0%, eaa.array#(i%))

' CH 2 = Eba
        er11.num% = AI.Read(1, 2, 1, value2%)
        er12.num% = AI.Scale(1, 1, value2%, eba.array#(i%))

' CH 4 = Ean
        er13.num% = AI.Read(1, 4, 1, value4%)
        er14.num% = AI.Scale(1, 1, value4%, ean.array#(i%))

' CH 6 = Ebn
        er15.num% = AI.Read(1, 6, 1, value6%)
        er16.num% = AI.Scale(1, 1, value6%, ebn.array#(i%))

er17.num% = CTR.EvRead (1, 1, overflo%, tcount%)

LWtotal! = LWtotal! + tcount%

NEXT i%

CLS:LOCATE 5,15:PRINT "Total Time is " LWtotal!*1E-6" seconds."

CALL Mean (eaa.array#(), 1000, eaa#)
CALL Mean (eba.array#(), 1000, eba#)
CALL Mean (ean.array#(), 1000, ean#)
CALL Mean (ebn.array#(), 1000, ebn#)


'*******************************************************************************

' This multiplication (*1000) will make the voltages in mV

eaa#=eaa#*1000
eba#=eba#*1000
ean#=ean#*1000
```

```
ebn#=ebn#*1000

END SUB


'**************************************************************************
'**************************************************************************


SUB forces (K#(),eaa#,eba#,ean#,ebn#,AX#,Max#,NORM#,Mnorm#,alpha#)

' FORCES AND MOMENTS CALCULATIONS (See thesis for explaination)

AX# = K#(1,1)*eaa# + K#(1,2)*eba# + K#(1,3)*ean# + K#(1,4)*ebn#
Max# = K#(2,1)*eaa# + K#(2,2)*eba# + K#(2,3)*ean# + K#(2,4)*ebn#
NORM# = K#(3,1)*eaa# + K#(3,2)*eba# + K#(3,3)*ean# + K#(3,4)*ebn#
Mnorm# = K#(4,1)*eaa# + K#(4,2)*eba# + K#(4,3)*ean# + K#(4,4)*ebn#

END SUB

'**************************************************************************
'**************************************************************************

SUB aero (AX#,NORM#,LIFT#,DRAG#,alpha#)

'**************************************************************************

PI# = 3.141593

LIFT# = NORM# * COS(PI#/180*alpha#) - AX# * SIN(PI#/180*alpha#)

DRAG# = NORM# * SIN(PI#/180*alpha#) + AX# * COS(PI#/180*alpha#)

END SUB

'**************************************************************************
'**************************************************************************
SUB tare (ean#,eaa#,ebn#,eba#,alpha#)
'**************************************************************************
'
' S/R to read Channel 0,2,4,6 on MC-MIO-16L-9 for Analog Voltage
```

```
'
'*************************************************************************

'  Setting Board code for MC-MIO-16L-9

board.code%=0

'*************************************************************************

CLS: LOCATE 5, 20: INPUT "Ready to take tare readings? (Y/N)"; T$

IF T$ <> "Y" THEN RETURN

err1.num% = Init.DA.Brds(1, board.code%)

err2.num% = AI.Setup(1, 0, 1)
err3.num% = AI.Setup(1, 2, 1)
err4.num% = AI.Setup(1, 4, 1)
err5.num% = AI.Setup(1, 6, 1)

' Configure and set clock to 1MHZ

err6.num% = CTR.Clock (1, 1, 1, 1)
err7.num% = CTR.Config (1, 1, 0, 0, 0, 0)

LWtotal! = 0

FOR i% = 1 TO 1000

err8.num% = CTR.EvCount (1, 1, 1, 0)

' CH 0 = Eaa
        err9.num% = AI.Read(1, 0, 1, value0%)
        er10.num% = AI.Scale(1, 1, value0%, eaa.array#(i%))

' CH 2 = Eba
        er11.num% = AI.Read(1, 2, 1, value2%)
        er12.num% = AI.Scale(1, 1, value2%, eba.array#(i%))

' CH 4 = Ean
        er13.num% = AI.Read(1, 4, 1, value4%)
```

```
        er14.num% = AI.Scale(1, 1, value4%, ean.array#(i%))

' CH 6 = Ebn
        er15.num% = AI.Read(1, 6, 1, value6%)
        er16.num% = AI.Scale(1, 1, value6%, ebn.array#(i%))

er17.num% = CTR.EvRead (1, 1, overflo%, tcount%)

LWtotal! = LWtotal! + tcount%

NEXT i%

CLS:LOCATE 5,15:PRINT "Total Time is " LWtotal!*1E-6" seconds."

CALL Mean (eaa.array#(), 1000, eaa#)
CALL Mean (eba.array#(), 1000, eba#)
CALL Mean (ean.array#(), 1000, ean#)
CALL Mean (ebn.array#(), 1000, ebn#)

'*****************************************************************************

' This multiplication (*1000) will make the voltages in mV

eaa#=eaa#*1000
eba#=eba#*1000
ean#=ean#*1000
ebn#=ebn#*1000

PRINT " "
PRINT "      AOA        EAA (mV)      EBA (mV)      EAN (mV)       EBN
(mV)"
PRINT "    **********      **********      **********      **********      **********"

PRINT USING "    ####.######";  alpha#; eaa#; eba#; ean#; ebn#
PRINT #1, USING "#####.######"; alpha#; eaa#; eba#; ean#; ebn#

END SUB
```

APPENDIX E: WIND TUNNEL DATA

Alpha=	22					
deltac=	4					
DeltaP (cm H2O)=	12					
Epsilon body=	0.01116328					
Epsilon body+canard=	0.01284224					
q (lbf/ft^2)=	27.3316484					
S (ft^2)	0.815					
V (ft/s2)=	151.650014					
Re=	7.69E+05					
Hz	0	5	10	15	20	25
k=	0	0.04645424	0.09290848	0.13936272	0.18581695	0.23227119
LIFT						
Mean	27.9649726	26.634203	26.696337	26.488675	26.382005	26.060466
Std. Dev.	0.20225274	0.12263605	0.19785138	0.19474272	0.20292163	0.20150568
1.96*Std. Dev.	0.39641537	0.24036666	0.3877887	0.38169574	0.3977264	0.39495114
High 95%	28.361388	26.8745697	27.0841257	26.8703707	26.7797314	26.4554171
Low 95%	27.5685573	26.3938363	26.3085483	26.1069793	25.9842786	25.6655149
Mean CL	1.22398806	1.16574212	1.16846164	1.15937256	1.15470377	1.14063045
1.96*CL Std. Dev.	0.00885232	0.00536761	0.00865968	0.00852362	0.0088816	0.00881962
DRAG						
Mean	10.5168105	10.324636	10.269471	10.164157	10.128822	10.006858
Standard Deviation	0.06405469	0.03671978	0.09930364	0.09534789	0.12415457	0.0273695
1.96*Std. Dev.	0.12554719	0.07197077	0.19463514	0.18688186	0.24334296	10.002575
High 95%	10.6423577	10.3966068	10.4641061	10.3510389	10.372165	0.08654996
Low 95%	10.3912633	10.2526652	10.0748359	9.97727514	9.88547904	0.16963791
Mean CD	0.46030621	0.451895	0.4494805	0.44487105	0.44332449	0.43798629
1.96*CD Std. Dev.	0.00280358	0.00160717	0.00434638	0.00417324	0.00543407	0.00119793

Alpha=	22					
deltac=	7					
DeltaP (cm H2O)=	12					
Epsilon body=	0.01116328					
Epsilon body+canard=	0.0130201					
q (lbf/ft^2)=	27.3316484					
S (ft^2)	0.815					
V (ft/s2)=	151.650014					
Re=	7.69E+05					
Hz	0	5	10	15	20	25
k=	0	0.04645424	0.092908477	0.13936272	0.18581695	0.23227119
LIFT						
Mean Lift	29.072835	29.4887185	29.7760765	29.83038	29.8068965	29.5474925
Standard Deviation	0.17436905	0.48544586	0.138682505	0.34246597	0.42561418	0.44659816
1.96 Std. Dev.	0.34176334	0.95147388	0.271817709	0.6712333	0.8342038	0.8753324
High 95%	29.4145983	30.4401924	30.04789421	30.5016133	30.6411003	30.4228249
Low 95%	28.7310717	28.5372446	29.50425879	29.1591467	28.9726927	28.6721601
Mean CL	1.27203651	1.29023284	1.30280574	1.3051817	1.30415422	1.2928044
1.96*CL Std. Dev.	0.00762925	0.02123993	0.006067836	0.01498406	0.01862208	0.01954021
DRAG						
Mean Drag	10.989402	11.061629	11.083714	11.059518	10.982303	10.916209
Standard Deviation	0.04131704	0.46697042	0.555855698	0.49225668	0.52967295	0.48248211
1.96* Std. Dev.	0.08098139	0.91526202	1.089477169	0.96482309	1.03815899	0.94566493
High 95%	11.0703834	11.976891	12.17319117	12.0243411	12.020462	11.8618739
Low 95%	10.9084206	10.146367	9.994236831	10.0946949	9.94414401	9.97054407
Mean CD	0.48082413	0.48398431	0.484950602	0.48389194	0.48051352	0.47762168
1.96*CD Std. Dev.	0.00180776	0.02043156	0.024320598	0.02153792	0.02317501	0.02111025

Alpha=	22					
Deltac=	10					
DeltaP (cm H2O)=	12					
Epsilon body=	0.01116328					
Epsilon body+canard=	0.01319287					
q (lbf/ft^2)=	27.3316484					
S (ft^2)	0.815					
V (ft/s2)=	151.650014					
Re=	7.69E+05					
Hz	0	5	10	15	20	25
k=	0	0.04643853	0.09287706	0.13931559	0.18575411	0.23219264
LIFT						
Mean Lift	26.6439583	27.600294	28.1596091	28.1582487	28.3246653	28.2241233
Standard Deviation	0.17054131	0.38256539	0.21255614	0.16470014	0.30089305	0.21897795
1.96*Std. Dev.	0.33426097	0.74982817	0.41661004	0.32281228	0.58975037	0.42919679
High 95%	26.9782193	28.3501222	28.5762191	28.4810609	28.9144157	28.6533201
Low 95%	26.3096974	26.8504658	27.742999	27.8354364	27.734915	27.7949265
Mean CL	1.16537234	1.20720122	1.23166494	1.23160544	1.23888429	1.23448671
1.96*CL Std. Dev.	0.01462014	0.03279652	0.01822199	0.01411939	0.02579492	0.01877251
DRAG						
Mean Drag	10.809935	11.050196	11.1340316	11.0934887	11.0961793	11.023988
Standard Deviation	0.04123263	0.18159774	0.22376169	0.23089359	0.2491573	0.21904721
1.96*Std. Dev.	0.08081595	0.35593158	0.43857291	0.45255143	0.48834832	0.42933254
High 95%	10.8907509	11.4061276	11.5726045	11.5460401	11.5845277	11.4533205
Low 95%	10.7291191	10.6942644	10.6954587	10.6409372	10.607831	10.5946555
Mean CD	0.4728126	0.48332131	0.48698816	0.48521487	0.48533256	0.482175
1.96*CD Std. Dev.	0.00353479	0.01556799	0.01918261	0.01979402	0.02135972	0.01877845

Alpha=	34					
Deltac=	-4					
DeltaP (cm H2O)=	12					
Epsilon body=	0.01666395					
Epsilon body+canard=	0.01857895					
q (lbf/ft^2)=	27.3316484					
S (ft^2)	0.815					
V (ft/s2)=	151.650014					
Re=	7.69E+05					
Hz	0	5	10	15	20	25
k=	0	0.04645424	0.09290848	0.13936272	0.18581695	0.23227119
LIFT						
Mean Lift	34.1584067	35.255284	35.323959	35.321435	35.166783	35.25195
Standard Deviation	0.27649726	0.16722914	0.13661708	0.18493793	0.16266148	0.17581846
1.96*Std. Dev.	0.54193462	0.32776911	0.26776947	0.36247834	0.31881651	0.34460418
High 95%	34.7003413	35.5830531	35.5917285	35.6839133	35.4855995	35.5965542
Low 95%	33.616472	34.9275149	35.0561895	34.9589567	34.8479665	34.9073458
Mean CL	1.47852711	1.52600482	1.52897738	1.52886813	1.5221741	1.52586051
1.96*CL Std. Dev.	0.02345733	0.0141873	0.01159025	0.01568967	0.01379979	0.01491599
DRAG						
Mean Drag	20.9137483	21.3962375	21.3841785	21.3600625	21.2802595	21.3368925
Standard Deviation	0.16485173	0.07953415	0.05839094	0.08142902	0.07376121	0.06714689
1.96*Std. Dev.	0.32310939	0.15588694	0.11444625	0.15960088	0.14457197	0.1316079
High 95%	21.2368577	21.5521244	21.4986247	21.5196634	21.4248315	21.4685004
Low 95%	20.5906389	21.2403506	21.2697323	21.2004616	21.1356875	21.2052846
Mean CD	0.90523964	0.92612391	0.92560195	0.9245581	0.92110387	0.9235552
1.96*CD Std. Dev.	0.01398561	0.00674748	0.00495374	0.00690823	0.00625771	0.00569657

Alpha=	34					
Deltac=	-7					
DeltaP (cm H2O)=	12					
Epsilon body=	0.01666395					
Epsilon body+canard=	0.01840273					
q (lbf/ft^2)=	27.3316484					
S (ft^2)	0.815					
V (ft/s2)=	151.650014					
Re=	7.69E+05					
Hz	0	5	10	15	20	25
k=	0	0.04645424	0.09290848	0.13936272	0.18581695	0.23227119
LIFT						
Mean Lift	34.9281845	34.3392823	34.4310765	34.3410235	34.4285855	34.4058575
Standard Deviation	0.21436019	0.22029783	0.16158673	0.10686481	0.14593063	0.14986457
1.96*Std. Dev.	0.42014597	0.43178374	0.31670999	0.20945503	0.28602404	0.29373456
High 95%	35.3483305	34.771066	34.7477865	34.5504785	34.7146095	34.6995921
Low 95%	34.5080385	33.9074986	34.1143665	34.1315685	34.1425615	34.1121229
Mean CL	1.51236041	1.48686145	1.49083606	1.48693685	1.49072821	1.4897441
1.96*CL Std. Dev.	0.01819196	0.01869587	0.01371327	0.00906922	0.0123846	0.01271845
DRAG						
Mean Drag	21.0848035	20.7696615	20.7546585	20.6869115	20.7280485	20.7817165
Standard Deviation	0.11526178	0.12368821	0.10170331	0.05490734	0.06544965	0.06620331
1.96*Std. Dev.	0.22591309	0.24242889	0.19933848	0.1076184	0.12828131	0.12975849
High 95%	21.3107166	21.0120904	20.953997	20.7945299	20.8563298	20.911475
Low 95%	20.8588905	20.5272327	20.55532	20.5792931	20.5997672	20.651958
Mean CD	0.9129539	0.89930852	0.8986589	0.89572551	0.89750671	0.89983049
1.96*CD Std. Dev.	0.00978184	0.01049696	0.00863119	0.00465978	0.00555447	0.00561843

Alpha=	34					
Deltac=	-10					
DeltaP (cm H2O)=	12					
Epsilon body=	0.01666395					
Epsilon body+canard=	0.01822175					
q (lbf/ft^2)=	27.3316484					
S (ft^2)	0.815					
V (ft/s2)=	151.650014					
Re=	7.69E+05					
Hz	0	5	10	15	20	25
k=	0	0.04645424	0.09290848	0.13936272	0.18581695	0.23227119
LIFT						
Mean Lift	34.657363	32.6935073	32.5251765	32.3101165	32.1713068	32.7273225
Standard Deviation	0.18474608	0.29195573	0.13795774	0.16674074	0.11750209	0.51619205
1.96*Std. Dev.	0.36210232	0.57223323	0.27039717	0.32681185	0.23030409	1.01173642
High 95%	35.0194653	33.2657405	32.7955737	32.6369284	32.4016109	33.7390589
Low 95%	34.2952607	32.121274	32.2547793	31.9833046	31.9410027	31.7155861
Mean CL	1.50115815	1.41609519	1.40880406	1.3994889	1.39347646	1.41755987
1.96*CL Std. Dev.	0.0156842	0.02478586	0.01171205	0.01415561	0.00997545	0.04382262
DRAG						
Mean Drag	20.5163945	19.0849359	18.97399	18.83677	18.7576423	19.216226
Standard Deviation	0.10018967	0.15470655	0.06094193	0.08007228	0.06362604	0.41955322
1.96*Std. Dev.	0.19637175	0.30322485	0.11944618	0.15694167	0.12470703	0.82232432
High 95%	20.7127662	19.3881608	19.0934362	18.9937117	18.8823493	20.0385503
Low 95%	20.3200228	18.7817111	18.8545438	18.6798283	18.6329352	18.3939017
Mean CD	0.88865252	0.82664994	0.8218444	0.81590082	0.81247346	0.83233668
1.96*CD Std. Dev.	0.0085057	0.01313396	0.00517372	0.00679781	0.00540159	0.03561837

Alpha	deltac	osc	Axial	Normal	Lift	Drag	L Drift	D Drift	LIFT	DRAG
f8_7a										
22	4	0	-0.0004	-0.00266	-0.00137	0.00232	2.12714	0.65282		
22	4	5	30.8934	0.57129	28.85788	11.04318			26.73074	10.39036
22	4	5	30.72504	0.5729	28.70238	10.97862			26.57524	10.3258
22	4	5	30.6268	0.5581	28.60575	10.95554			26.47861	10.30272
22	4	5	30.6751	0.55772	28.65038	10.97399			26.52324	10.32117
22	4	5	30.6912	0.58026	28.67375	10.95911			26.54661	10.30629
22	4	10	31.11129	0.64319	29.08683	11.05814			26.95969	10.40532
22	4	10	30.82153	0.63944	28.81676	10.95307			26.68962	10.30025
22	4	10	31.07847	0.66481	29.0645	11.0258			26.93736	10.37298
22	4	10	30.89822	0.63316	28.88552	10.98762			26.75838	10.3348
22	4	10	31.08931	0.66161	29.07335	11.03283			26.94621	10.38001
22	4	15	30.81608	0.67392	28.82463	10.91906			26.69749	10.26624
22	4	15	30.82892	0.68327	28.84004	10.9152			26.7129	10.26238
22	4	15	30.70886	0.66342	28.72128	10.88863			26.59414	10.23581
22	4	15	30.66375	0.65564	28.67654	10.87894			26.5494	10.22612
22	4	15	30.74675	0.65825	28.75448	10.90762			26.62734	10.2548
22	4	20	30.77101	0.64179	28.7708	10.93197			26.64366	10.27915
22	4	20	30.67964	0.64899	28.68878	10.89106			26.56164	10.23824
22	4	20	30.79199	0.66727	28.7998	10.9162			26.67266	10.26338
22	4	20	30.50452	0.61326	28.51303	10.85859			26.38589	10.20577
22	4	20	30.61783	0.62731	28.62335	10.88801			26.49621	10.23519
22	4	25	30.45834	0.69268	28.49996	10.76765			26.37282	10.11483
22	4	25	30.4239	0.66037	28.45593	10.78471			26.32879	10.13189
22	4	25	30.27619	0.67288	28.32366	10.71778			26.19652	10.06496
22	4	25	30.24848	0.66854	28.29635	10.71142			26.16921	10.0586
22	4	25	30.1811	0.64727	28.2259	10.7059			26.09876	10.05308
22	4	0	2.24596	0.2116	2.16168	0.64516				
22	4	0	2.18764	0.17151	2.0926	0.66048				
f8_7b										
22	4	0	0.00356	0.00895	0.00665	-0.00696	1.75124	0.20049		
22	4	5	31.60487	1.07245	29.70527	10.84503			27.95403	10.64454
22	4	5	31.57332	1.05455	29.66931	10.84981			27.91807	10.64932
22	4	5	31.44743	1.03871	29.54666	10.81734			27.79542	10.61685
22	4	5	31.66408	1.06643	29.75792	10.87279			28.00668	10.6723
22	4	5	31.59037	1.06055	29.68737	10.85063			27.93613	10.65014
22	4	10	31.10655	1.11469	29.25907	10.61919			27.50783	10.4187
22	4	10	31.14534	1.12131	29.2975	10.62759			27.54626	10.4271
22	4	10	31.26848	1.12196	29.41192	10.67312			27.66068	10.47263
22	4	10	31.20717	1.11853	29.35379	10.65333			27.60255	10.45284
22	4	10	31.12222	1.12039	29.27572	10.61978			27.52448	10.41929
22	4	15	30.93429	1.14065	29.10907	10.53059			27.35783	10.3301
22	4	15	30.86193	1.14563	29.04384	10.49887			27.2926	10.29838

22	4	20	30.73065	1.13913	28 91969	10 45572				27.16845	10 25523
22	4	20	30 89981	1.17741	29 09087	10 48359				27.33963	10 2831
22	4	20	30 75962	1.15808	28 95365	10.449				27.20241	10 24851
22	4	20	30 84409	1.16079	29 03298	10 47813				27.28174	10 27764
22	4	25	30.61381	1.14735	28 81444	10.40434				27.0632	10.20385
22	4	25	30 57054	1.1489	28.77489	10 38669				27.02365	10.1862
22	4	25	30 60389	1.14837	28 80562	10 39967				27 05438	10.19918
22	4	25	30 39866	1.11887	28 60428	10 35014				26 85304	10 14965
22	4	25	30 37517	1.14022	28 5905	10 32155				26 83926	10.12106
22	4	0	1.70479	0.47325	1.75794	0.19984					
22	4	0	1 69286	0 46702	1.74454	0 20114					
f8_7c											
22	4	0	-0 00731	0 00333	-0 00553	-0.00582	0.98391	0 31256			
22	4	5	29 82355	0 52032	27 84683	10.68966				26 86292	10.3771
22	4	5	29 5677	0 52008	27.60952	10 59405				26 62561	10 28149
22	4	5	29 54302	0 49852	27.57856	10 60479				26.59465	10 29223
22	4	5	29.74525	0 51759	27.7732	10 66286				26.78929	10 3503
22	4	5	29 56449	0 5	27.59903	10 61146				26 61512	10.2989
22	4	10	29 34064	0 57582	27.41988	10 45731				26 43597	10.14475
22	4	10	29 49516	0 58851	27.56789	10.50343				26 58398	10.19087
22	4	10	29 37618	0 55989	27.44686	10.48539				26 46295	10.17283
22	4	10	29 54804	0 5884	27 61689	10 52334				26 63298	10.21078
22	4	10	29 46615	0 58622	27.54014	10 49468				26 55623	10.18212
22	4	15	29 2585	0 58675	27 3478	10 4164				26 36389	10.10384
22	4	15	28 99486	0.58473	27 10261	10.31951				26.1187	10.00695
22	4	15	29 33384	0 62467	27 43187	10 40947				26.44796	10 09691
22	4	15	29.41751	0 62794	27.51067	10.43778				26.52676	10 12522
22	4	15	29 13602	0 58098	27.23208	10 37586				26.24817	10.0633
22	4	20	29 15985	0 6179	27.26802	10.35057				26 28411	10 03801
22	4	20	29 09196	0 61412	27 20365	10.32864				26.21974	10.01608
22	4	20	29 15347	0 62679	27.26542	10.33993				26 28151	10.02737
22	4	20	29 06519	0 61331	27.17852	10.31936				26.19461	10 0068
22	4	20	28 94823	0 59687	27.06393	10 29079				26 08002	9.97823
22	4	25	28.75715	0 574	26 87819	10.24041				25 89428	9.92785
22	4	25	28.6414	0 56119	26.76607	10.20893				25 78216	9 89637
22	4	25	28.77493	0 57566	26 89529	10 24553				25.91138	9 93297
22	4	25	28.77813	0 57374	26 89755	10.24852				25.91364	9.93596
22	4	25	28 80592	0 56759	26 92101	10 26463				25.9371	9 95207
22	4	0	1.02482	0 06758	0 97552	0.32124					
22	4	0	1.03388	0 08997	0.9923	0.30388					

Alpha	deltac	osc	Axial	Normal	Lift	Drag	L Drift	D Drift	LIFT	DRAG
f8_5a										
22	7	0	-0.00109	0.00395	0.00047	-0.00408	0.285755	0.079915		
22	7	5	31.49671	0.2453	29.29513	11.57143			29.009375	11.491515
22	7	5	31.44597	0.21917	29.2383	11.57665			28.952545	11.496735
22	7	5	31.49265	0.23083	29.28594	11.58333			29.000185	11.503415
22	7	5	31.58435	0.24435	29.37603	11.60515			29.090275	11.525235
22	7	5	31.60648	0.27864	29.4094	11.58165			29.123645	11.501735
22	7	10	32.22642	0.38896	30.02552	11.71159			29.739765	11.631675
22	7	10	32.04333	0.38932	29.85591	11.64267			29.570155	11.562755
22	7	10	32.22018	0.38172	30.01702	11.71597			29.731265	11.636055
22	7	10	32.05315	0.36128	29.8545	11.67234			29.568745	11.592425
22	7	10	32.19703	0.37958	29.99476	11.70928			29.709005	11.629365
22	7	15	31.88008	0.38615	29.70335	11.58445			29.417595	11.504535
22	7	15	32.08673	0.41135	29.90439	11.6385			29.618635	11.558585
22	7	15	32.0063	0.4236	29.83441	11.59701			29.548655	11.517095
22	7	15	31.94974	0.401	29.7735	11.59679			29.487745	11.516875
22	7	15	32.00196	0.4087	29.82481	11.60921			29.539055	11.529295
22	7	20	31.89557	0.40604	29.72516	11.57182			29.439405	11.491905
22	7	20	31.88365	0.39022	29.70819	11.58202			29.422435	11.502105
22	7	20	31.84485	0.40663	29.67836	11.55227			29.392605	11.472355
22	7	20	31.98668	0.41637	29.81351	11.59637			29.527755	11.516455
22	7	20	31.70842	0.38722	29.54459	11.51916			29.258835	11.439245
22	7	25	31.72226	0.42376	29.57111	11.49046			29.285355	11.410545
22	7	25	31.48607	0.38885	29.33904	11.43436			29.053285	11.354445
22	7	25	31.62611	0.38939	29.46908	11.48631			29.183325	11.406395
22	7	25	31.66855	0.42063	29.52014	11.47325			29.234385	11.393335
22	7	25	31.34769	0.39356	29.2125	11.37815			28.926745	11.298235
22	7	0	0.29848	0.02706	0.28689	0.08672				
22	7	0	0.29128	0.03883	0.28462	0.07311				
f8_5b										
22	7	0	-0.00289	0.00092	-0.00233	-0.00193	-0.31153	0.422625		
22	7	5	31.62239	0.85403	29.6397	11.05411			29.95123	10.631485
22	7	5	31.74301	0.84543	29.74831	11.10727			30.05984	10.684645
22	7	5	31.45243	0.85142	29.48113	10.99286			29.79266	10.570235
22	7	5	31.55979	0.8463	29.57876	11.03783			29.89029	10.615205
22	7	5	31.67024	0.91155	29.70561	11.01871			30.01714	10.596085
22	7	10	31.57287	0.91538	29.61676	10.97867			29.92829	10.556045
22	7	10	31.61056	0.89143	29.64274	11.01501			29.95427	10.592385
22	7	10	31.50778	0.9	29.55065	10.96856			29.86218	10.545935
22	7	10	31.43392	0.88801	29.47768	10.952			29.78921	10.529375
22	7	10	31.55584	0.90303	29.59635	10.98375			29.90788	10.561125
22	7	15	31.97054	0.99114	30.01386	11.0574			30.32539	10.634775
22	7	15	31.78404	0.94672	29.82429	11.02873			30.13582	10.606105

22	7	20	31.81819	1.08922	29.90934	10.90939				30.22087	10.486765
22	7	20	31.79633	1.0915	29.88992	10.89909				30.20145	10.476465
22	7	20	31.8382	1.09485	29.93001	10.91168				30.24154	10.489055
22	7	20	31.76851	1.088	29.86282	10.89192				30.17435	10.469295
22	7	25	31.61882	1.02409	29.70009	10.89509				30.01162	10.472465
22	7	25	31.54746	1.02353	29.63372	10.86889				29.94525	10.446265
22	7	25	31.55105	1.00346	29.62952	10.88884				29.94105	10.466215
22	7	25	31.65665	1.0143	29.73149	10.91835				30.04302	10.495725
22	7	25	31.44956	1.01396	29.53936	10.84109				29.85089	10.418465
22	7	0	-0.13181	-0.5148	-0.31506	0.42793					
22	7	0	-0.12924	-0.50231	-0.308	0.41732					
f8_5c											
22	7	0	-0.00091	0.00372	0.00055	-0.00379	1.020925	0.284715			
22	7	5	31.43877	0.29864	29.26139	11.50027				28.240465	11.215555
22	7	5	31.42313	0.3203	29.25501	11.47434				28.234085	11.189625
22	7	5	31.37038	0.3144	29.20388	11.46004				28.182955	11.175325
22	7	5	31.21911	0.30442	29.05989	11.41263				28.038965	11.127915
22	7	5	31.29848	0.33332	29.1443	11.41557				28.123375	11.130855
22	7	10	31.27879	0.42183	29.15921	11.32613				28.138285	11.041415
22	7	10	31.43151	0.43474	29.30565	11.37137				28.284725	11.086655
22	7	10	31.53156	0.46197	29.40861	11.3836				28.387685	11.098885
22	7	10	31.4618	0.44955	29.33928	11.36898				28.318355	11.084265
22	7	10	31.24836	0.44212	29.1386	11.29591				28.117675	11.011195
22	7	15	31.45977	0.50134	29.3568	11.3202				28.335875	11.035485
22	7	15	31.26735	0.50539	29.1799	11.24437				28.158975	10.959655
22	7	15	31.20401	0.49701	29.11804	11.22841				28.097115	10.943695
22	7	15	31.25766	0.50328	29.17012	11.24269				28.149195	10.957975
22	7	15	31.40891	0.52316	29.31781	11.28092				28.296885	10.996205
22	7	20	31.40136	0.66362	29.36343	11.14786				28.342505	10.863145
22	7	20	31.12683	0.6466	29.10252	11.0608				28.081595	10.776085
22	7	20	31.27	0.6752	29.24597	11.08791				28.225045	10.803195
22	7	20	31.2123	0.6466	29.18176	11.09281				28.160835	10.808095
22	7	20	31.24629	0.65725	29.21727	11.09568				28.196345	10.810965
22	7	25	31.02023	0.6419	29.00191	11.02522				27.980985	10.740505
22	7	25	31.17411	0.66387	29.15282	11.0625				28.131895	10.777785
22	7	25	30.97539	0.65137	28.96389	10.99965				27.942965	10.714935
22	7	25	30.99137	0.666	28.98419	10.99207				27.963265	10.707355
22	7	25	31.14076	0.67923	29.12765	11.03576				28.106725	10.751045
22	7	0	1.05283	0.127	1.01876	0.29447					
22	7	0	1.0516	0.12832	1.02309	0.27496					

Alpha	deltac	osc	Axial	Normal	Lift	Drag	L Drift	D Drift	LIFT	DRAG
f8_6a										
22	10	0	0.00092	-0.00089	0.00052	0.00117	0.96182	0.06688		
22	10	5	30.86767	0.11394	28.66269	11.45759			27.70087	11.39071
22	10	5	30.63252	0.09817	28.43876	11.38412			27.47694	11.31724
22	10	5	30.50693	0.09715	28.32193	11.33802			27.36011	11.27114
22	10	5	30.48161	0.11834	28.30639	11.30889			27.34457	11.24201
22	10	5	30.37664	0.08794	28.19768	11.29775			27.23586	11.23087
22	10	10	31.30138	0.23129	29.10878	11.51126			28.14696	11.44438
22	10	10	31.54859	0.25406	29.34652	11.58275			28.3847	11.51587
22	10	10	31.38128	0.23789	29.18534	11.53506			28.22352	11.46818
22	10	10	31.19252	0.22273	29.00464	11.47842			28.04282	11.41154
22	10	10	31.17298	0.21939	28.98527	11.47419			28.02345	11.40731
22	10	15	31.4148	0.32106	29.24757	11.47051			28.28575	11.40363
22	10	15	31.46266	0.31298	29.28892	11.49593			28.3271	11.42905
22	10	15	31.33074	0.29623	29.16032	11.46204			28.1985	11.39516
22	10	15	31.31987	0.29637	29.15029	11.45784			28.18847	11.39096
22	10	15	31.35292	0.30816	29.18535	11.45929			28.22353	11.39241
22	10	20	31.729	0.45731	29.58993	11.46188			28.62811	11.395
22	10	20	31.82264	0.47484	29.68332	11.4807			28.7215	11.41382
22	10	20	31.75818	0.46664	29.62047	11.46416			28.65865	11.39728
22	10	20	31.82038	0.45586	29.67411	11.49746			28.71229	11.43058
22	10	20	32.00811	0.46846	29.85289	11.55609			28.89107	11.48921
22	10	25	31.50517	0.46242	29.38431	11.3733			28.42249	11.30642
22	10	25	31.4367	0.47578	29.32584	11.33526			28.36402	11.26838
22	10	25	31.71917	0.47458	29.58728	11.44219			28.62546	11.37531
22	10	25	31.58094	0.47486	29.45922	11.39014			28.4974	11.32326
22	10	25	31.60903	0.48572	29.48933	11.3906			28.52751	11.32372
22	10	0	0.92687	0.29923	0.97147	0.06977				
22	10	0	0.9068	0.29736	0.95217	0.06399				
f8_6b										
22	10	0	-0.0023	0.00032	-0.00201	-0.00115	2.067945	-0.752845		
22	10	5	30.90938	1.55065	29.23956	10.14112			27.171615	10.893965
22	10	5	31.01703	1.56117	29.34332	10.17169			27.275375	10.924535
22	10	5	31.16244	1.55934	29.47745	10.22786			27.409505	10.980705
22	10	5	30.9101	1.58684	29.25379	10.10783			27.185845	10.860675
22	10	5	31.13463	1.59155	29.46373	10.18758			27.395785	10.940425
22	10	10	31.57863	1.69579	29.91445	10.25725			27.846505	11.010095
22	10	10	31.77246	1.72015	30.10329	10.30728			28.035345	11.060125
22	10	10	31.5619	1.69705	29.89941	10.24981			27.831465	11.002655
22	10	10	31.73422	1.70115	30.06072	10.31057			27.992775	11.063415
22	10	10	31.61208	1.71672	29.9533	10.25038			27.885355	11.003225
22	10	15	31.58487	1.76589	29.94649	10.19459			27.878545	10.947435
22	10	15	31.70871	1.76631	30.06148	10.2406			27.993535	10.993445

22	10	20	31.77684	1.79489	30 13535	10 23962			28 067405	10.992465
22	10	20	31 86339	1 80167	30 21814	10 26576			28 150195	11.018605
22	10	20	31.92102	1.82439	30 28008	10 26628			28.212135	11.019125
22	10	20	31 86617	1.81451	30 22553	10.25489			28.157585	11.007735
22	10	25	31 93175	1.94208	30 33412	10.16118			28.266175	10.914025
22	10	25	31.89215	1.92275	30.29016	10.16427			28.222215	10.917115
22	10	25	31.78953	1.94755	30 2043	10.10283			28.136355	10.855675
22	10	25	31.82513	1.94615	30.23679	10.11746			28.168845	10 870305
22	10	25	31.63435	1 93053	30.05405	10.06048			27.986105	10 813325
22	10	0	1.63729	1.46975	2.06864	-0.74939				
22	10	0	1.63341	1.47563	2 06725	-0 7563				
f8_6c										
22	10	0	-0.00406	-0 00248	-0 0047	0 00078	0.421025	0 005755		
22	10	5	30 53257	0 53828	28.51095	10 93861			28 089925	10 932855
22	10	5	30.4149	0.51225	28.3921	10 91867			27.971075	10.912915
22	10	5	30 48286	0 52808	28.46103	10 92945			28 040005	10.923695
22	10	5	30 59938	0.54198	28.57427	10 96022			28.153245	10.954465
22	10	5	30 64521	0.53647	28 61471	10.98249			28.193685	10 976735
22	10	10	30 68783	0.58671	28 67304	10 95187			28.252015	10.946115
22	10	10	30 88982	0 61241	28 86996	11.00371			28 448935	10.997955
22	10	10	30.70482	0 61004	28 69754	10.93661			28 276515	10 930855
22	10	10	30 8647	0 62823	28 85259	10 97964			28.431565	10.973885
22	10	10	30.76877	0 61945	28 76035	10 95184			28.339325	10.946085
22	10	10	30.82433	0 62385	28 81352	10 96857			28 392495	10.962815
22	10	15	30.79338	0 6305	28.78731	10 95082			28 366285	10 945065
22	10	15	30 54967	0 63665	28 56366	10.85382			28.142635	10 848065
22	10	15	30 60519	0 64456	28.6181	10 86728			28.197075	10.861525
22	10	15	30 77795	0 65075	28.78059	10 92626			28.359565	10 920505
22	10	15	30 68406	0 63866	28 68901	10 9023			28.267985	10 896545
22	10	20	30 53849	0 61724	28.54601	10.86763			28.124985	10 861875
22	10	20	30 57602	0 62464	28 58359	10 87483			28.162565	10 869075
22	10	20	30 43116	0 61426	28 44538	10 83018			28.024355	10 824425
22	10	20	30 57068	0 62202	28 57765	10.87525			28.156625	10 869495
22	10	20	30 60457	0 61163	28 60518	10 89758			28.184155	10.891825
22	10	25	30 53968	0 57287	28.5305	10.90921			28 109475	10.903455
22	10	25	30.39812	0 55792	28.39364	10 87005			27.972615	10.864295
22	10	25	30.54762	0 56399	28 53453	10.92041			28.113505	10.914655
22	10	25	30.435	0.56692	28.43121	10 87552			28.010185	10 869765
22	10	25	30.35835	0 56793	28 36052	10.84587			27.939495	10.840115
22	10	0	0 39574	0.14839	0 42251	0.01066				
22	10	0	0 38931	0 15638	0.41954	0 00085				

Alpha	dellac	osc	Axial	Normal	Lift	Drag	L Drift	D Drift	LIFT	DRAG
f8_13a										
34	-4	0	-0 00899	-0 00201	-0 00858	-0 00336	-0 187825	-0 053385		
34	-4	5	40 80264	1.85606	34 86482	21.2778			35.052645	21.331185
34	-4	5	40 80081	1 88238	34 87802	21.25496			35 065845	21.308345
34	-4	5	40 98173	1 89972	35 0377	21.34175			35 225525	21.395135
34	-4	5	40.76993	1.889	34 85612	21.2322			35 043945	21.285585
34	-4	5	41.03707	1.90037	35 08395	21.37217			35 271775	21.425555
34	-4	10	41.12875	1.9251	35 17378	21.40292			35.361605	21.456305
34	-4	10	40.99873	1.93915	35 07385	21.31857			35.261675	21.371955
34	-4	10	40 99357	1 94513	35 07292	21.31073			35.260745	21.364115
34	-4	10	40.96896	1.93696	35 04794	21.30374			35.235765	21.357125
34	-4	10	40.76398	1.90366	34.85939	21.21673			35.047215	21.270115
34	-4	15	40 93724	1.95555	35.03204	21.27059			35.219865	21.323975
34	-4	15	40.79001	1.92914	34 89521	21.21015			35.083035	21.263535
34	-4	15	40 97183	1.95359	35.05962	21.29156			35.247445	21.344945
34	-4	15	40.87551	1.92919	34 96612	21.25792			35.153945	21.311305
34	-4	15	40.8577	1.95336	34 96487	21.22793			35.152695	21 281315
34	-4	20	40 65379	1.90642	34 76957	21.15282			34 957395	21.206205
34	-4	20	40 89142	1.92519	34 97708	21 27014			35.164905	21.323525
34	-4	20	40.96117	1.96	35 05436	21.28028			35 242185	21.333665
34	-4	20	40.63801	1 91652	34.76214	21.13562			34 949965	21.189005
34	-4	20	40 65289	1 93853	34.78679	21.12569			34 974615	21 179075
34	-4	25	40 91932	1 92256	34 99873	21 28792			35.186555	21.341305
34	-4	25	40.79645	1.92539	34 89845	21.21687			35 086275	21.270255
34	-4	25	40 93164	1.93887	35 01806	21 28129			35.205885	21.334675
34	-4	25	40 8146	1.9302	34 91619	21.22303			35.104015	21.276415
34	-4	25	40.67603	1.89387	34.78099	21 17566			34.968815	21.229045
34	-4	0	-0.18181	-0.06296	-0.18594	-0 04947				
34	-4	0	-0.18932	-0.05858	-0.18971	-0.0573				
f8_13b	-4	0	-0 00662	-0 00198	-0 0066	-0 00206	-0 260935	0 06422		
34	-4	5	41.30925	1.8033	35 25531	21.60483			35 516245	21 54061
34	-4	5	40 94254	1.79521	34 94677	21.40648			35 207705	21.34226
34	-4	5	41.14993	1.8244	35.13503	21.49826			35.395965	21.43404
34	-4	5	41.20146	1.81396	35.17191	21.53572			35.432845	21.4715
34	-4	5	41.10053	1.79817	35.07941	21.49238			35.340345	21.42816
34	-4	10	41.27489	1.87305	35.26583	21.52779			35.526765	21.46357
34	-4	10	41.16147	1 86452	35.16703	21.47144			35 427965	21.40722
34	-4	10	41.13973	1.86265	35.14797	21.46084			35.408905	21.39662
34	-4	10	40.99092	1.84015	35.01201	21.39628			35.272945	21.33206
34	-4	10	41.17679	1.85619	35.17507	21.48692			35.436005	21.4227
34	-4	15	41.21833	1.87807	35.22175	21.49201			35.482685	21.42779
34	-4	15	41.38276	1.89331	35.36659	21.57132			35.627525	21.5071
34	-4	15	40 97503	1.87433	35.01795	21.35906			35.278885	21.29484

34	-4	20	41 00938	1 84881	35 03216	21.39942				35 293095	21.3352
34	-4	20	40 91813	1.85923	34 96234	21.33976				35 223275	21.27554
34	-4	20	40 83805	1 84293	34 88683	21 30849				35.147765	21.24427
34	-4	25	41 08215	1.84303	35 08926	21.4449				35 350195	21.38068
34	-4	25	41.15739	1 87217	35.16792	21 46282				35 428855	21.3986
34	-4	25	41.11944	1 86556	35 13276	21.44708				35.393695	21.38286
34	-4	25	40 96526	1 8519	34 99731	21 37219				35 258245	21.30797
34	-4	25	41.27414	1 8924	35 27603	21.51134				35 536965	21.44712
34	-4	0	-0.16201	-0 19554	-0 24365	0 07151					
34	-4	0	-0.19882	-0 20278	-0 27822	0 05693					

Alpha	dellac	osc	Axial	Normal	Lift	Drag	L Drift	D Drift	LIFT	DRAG
f8_13c										
34	-7	0	0.0033	0.00047	0.003	0.00145	0.022575	0.258705		
34	-7	5	40.13722	1.73437	34.24511	21.00659			34.222535	20.747885
34	-7	5	40.04594	1.75497	34.18096	20.93847			34.158385	20.679765
34	-7	5	39.61469	1.71998	33.80387	20.72633			33.781295	20.467625
34	-7	5	40.40661	1.78067	34.49433	21.11885			34.471755	20.860145
34	-7	5	40.38094	1.78951	34.478	21.09717			34.455425	20.838465
34	-7	5	40.62715	1.79716	34.68639	21.2285			34.663815	20.969795
34	-7	5	40.25383	1.76932	34.36133	21.04283			34.338755	20.784125
34	-7	5	40.5343	1.80588	34.61429	21.16935			34.591715	20.910645
34	-7	10	40.47728	1.83386	34.58267	21.11427			34.560095	20.855565
34	-7	10	40.55576	1.84371	34.65323	21.14999			34.630655	20.891285
34	-7	10	40.36536	1.82057	34.48245	21.0627			34.459875	20.803995
34	-7	10	39.98679	1.80309	34.15883	20.8655			34.136255	20.606795
34	-7	10	40.57502	1.86013	34.67838	21.14715			34.655805	20.888445
34	-7	15	40.15373	1.84636	34.32142	20.92297			34.298845	20.664265
34	-7	15	40.08999	1.81172	34.24921	20.91606			34.226635	20.657355
34	-7	15	40.25393	1.84093	34.40145	20.98351			34.378875	20.724805
34	-7	15	40.18506	1.83675	34.34202	20.94847			34.319445	20.689765
34	-7	15	40.03943	1.83451	34.22004	20.86888			34.197465	20.610175
34	-7	20	40.03208	1.8262	34.2093	20.87167			34.186725	20.612965
34	-7	20	40.19731	1.84069	34.35438	20.95205			34.331805	20.693345
34	-7	20	40.18157	1.82281	34.33133	20.95808			34.308755	20.699375
34	-7	20	40.26053	1.85674	34.41577	20.97409			34.393195	20.715385
34	-7	20	40.30517	1.85801	34.45349	20.998			34.430915	20.739295
34	-7	25	40.19321	1.77491	34.3142	21.00429			34.291625	20.745585
34	-7	25	40.22968	1.77445	34.34417	21.02507			34.321595	20.766365
34	-7	25	40.10017	1.76281	34.2303	20.96229			34.207725	20.703585
34	-7	25	40.16322	1.77982	34.29208	20.98345			34.269505	20.724745
34	-7	25	40.38527	1.80649	34.49108	21.0855			34.468505	20.826795
34	-7	0	0.17704	-0.20209	0.03376	0.26654				
34	-7	0	0.14972	-0.20161	0.01139	0.25087				
f8_13d										
34	-7	0	-0.00682	-0.00029	-0.00582	-0.00358	0.03724	0.01127		
34	-7	5	40.04246	2.00198	34.3162	20.73174			34.27896	20.72047
34	-7	5	40.05971	2.01063	34.33533	20.73422			34.29809	20.72295
34	-7	5	40.25179	2.02152	34.50067	20.8326			34.46343	20.82133
34	-7	5	40.05417	2.02158	34.33686	20.72204			34.29962	20.71077
34	-7	5	40.16055	2.01993	34.42413	20.7829			34.38689	20.77163
34	-7	10	40.09504	2.06568	34.39541	20.70834			34.35817	20.69707
34	-7	10	40.06343	2.06786	34.37042	20.68885			34.33318	20.67758
34	-7	10	40.18907	2.0779	34.48019	20.75079			34.44295	20.73952
34	-7	10	39.99574	2.0637	34.31198	20.65445			34.27474	20.64318

34	-7	15	39 93206	2 06197	34 25822	20 62027				34 22098	20 609
34	-7	15	40 16436	2 08077	34 46132	20.73459				34 42408	20.72332
34	-7	20	40 28706	2 09595	34.57153	20.79062				34 53429	20 77935
34	-7	20	40 41792	2 1196	34 69324	20 84419				34 656	20 83292
34	-7	20	40.37185	2.1219	34 65633	20.81652				34 61909	20 80525
34	-7	20	40 07092	2.0822	34.38465	20.68115				34 34741	20 66988
34	-7	20	40.21405	2.10294	34.51491	20.74399				34 47767	20.73272
34	-7	25	40.22057	2 03984	34.48503	20.79995				34 44779	20.78868
34	-7	25	40.26361	2 05194	34 52747	20 81399				34 49023	20 80272
34	-7	25	40.29631	2.03867	34 54716	20.84328				34.50992	20 83201
34	-7	25	40 0841	2 04312	34 37372	20.72092				34.33648	20.70965
34	-7	25	40 51404	2 08297	34 75244	20 9283				34 7152	20 91703
34	-7	0	0 05365	0 02044	0 05591	0 01306					
34	-7	0	0 03754	0.00435	0.03355	0 01738					
34	-7	0	0 02034	0 00965	0 02226	0.00337					

Alpha	deltac	osc	Axial	Normal	Lift	Drag	L Drift	D Drift	LIFT	DRAG
f9_2b										
34	-10	0	0.00295	0.00648	0.00607	-0.00372	-0.17234	-0.047205		
34	-10	5	37.32882	2.35437	32.26354	18.92215			32.43588	18.969355
34	-10	5	37.50764	2.39561	32.43485	18.98795			32.60719	19.035155
34	-10	5	37.44065	2.39327	32.37801	18.95243			32.55035	18.999635
34	-10	5	37.09549	2.36349	32.0752	18.78411			32.24754	18.831315
34	-10	5	37.29397	2.37092	32.2439	18.88894			32.41624	18.936145
34	-10	10	37.34981	2.3858	32.29852	18.90783			32.47086	18.955035
34	-10	10	37.20786	2.36796	32.17086	18.84325			32.3432	18.890455
34	-10	10	37.18365	2.3606	32.14668	18.83581			32.31902	18.883015
34	-10	10	37.3324	2.38317	32.28261	18.90027			32.45495	18.947475
34	-10	10	37.55927	2.42755	32.49551	18.99034			32.66785	19.037545
34	-10	15	36.79708	2.34445	31.81716	18.63303			31.9895	18.680235
34	-10	15	37.08484	2.39437	32.08364	18.75255			32.25598	18.799755
34	-10	15	37.16865	2.3767	32.14325	18.81407			32.31559	18.861275
34	-10	15	36.91761	2.34651	31.91824	18.69872			32.09058	18.745925
34	-10	15	37.17294	2.39559	32.15736	18.80081			32.3297	18.848015
34	-10	20	36.91278	2.35409	31.91847	18.68974			32.09081	18.736945
34	-10	20	37.07438	2.38414	32.06925	18.75519			32.24159	18.802395
34	-10	20	37.00784	2.40391	32.02514	18.70159			32.19748	18.748795
34	-10	20	36.89685	2.37912	31.91926	18.66008			32.0916	18.707285
34	-10	20	36.80487	2.36838	31.837	18.61755			32.00934	18.664755
34	-10	20	36.79094	2.35556	31.81828	18.62039			31.99062	18.667595
34	-10	25	36.81366	2.33401	31.82507	18.65096			31.99741	18.698165
34	-10	25	37.13314	2.36631	32.10799	18.80283			32.28033	18.850035
34	-10	25	37.32177	2.40349	32.28516	18.87748			32.4575	18.924685
34	-10	25	37.1873	2.3656	32.15249	18.8337			32.32483	18.880905
34	-10	25	37.05544	2.34193	32.02995	18.77959			32.20229	18.826795
34	-10	0	-0.16835	-0.05487	-0.17025	-0.04865			0.00209	-0.001445
34	-10	0	-0.17019	-0.0596	-0.17443	-0.04576			-0.00209	0.001445
f9_2c										
34	-10	0	0.00196	0.0013	0.00235	0.00002	-0.084565	-0.032395		
34	-10	5	37.83676	2.45333	32.73998	19.12414			32.824545	19.156535
34	-10	5	38.2621	2.51239	33.12563	19.31303			33.210195	19.345425
34	-10	5	37.77113	2.43808	32.67704	19.10008			32.761605	19.132475
34	-10	5	38.14484	2.48568	33.01348	19.2696			33.098045	19.301995
34	-10	5	37.86552	2.46003	32.76757	19.13468			32.852135	19.167075
34	-10	5	37.61676	2.42238	32.54029	19.02679			32.624855	19.059185
34	-10	10	37.62272	2.46968	32.57168	18.9909			32.656245	19.023295
34	-10	10	37.69141	2.46421	32.62556	19.03385			32.710125	19.066245
34	-10	10	37.55301	2.45371	32.50496	18.96515			32.589525	18.997545
34	-10	10	37.55909	2.45807	32.51243	18.96495			32.596995	18.997345
34	-10	10	37.40044	2.41788	32.35843	18.90955			32.442995	18.941945

34	-10	15	37.29648	2.45331	32.29206	18.82204			32.376625	18.854435
34	-10	20	37.06977	2.42369	32.08754	18.71982			32.172105	18.752215
34	-10	20	37.20507	2.43098	32.20379	18.78944			32.288355	18.821835
34	-10	20	37.30727	2.441	32.29412	18.83828			32.378685	18.870675
34	-10	20	37.09243	2.42713	32.10826	18.72964			32.192825	18.762035
34	-10	20	37.14503	2.41737	32.1464	18.76714			32.230965	18.799535
34	-10	25	38.46036	2.23433	33.1345	19.65442			33.219065	19.686815
34	-10	25	38.28902	2.22655	32.98811	19.56505			33.072675	19.597445
34	-10	25	38.52346	2.2556	33.19871	19.67207			33.283275	19.704465
34	-10	25	38.49261	2.25935	33.17523	19.65171			33.259795	19.684105
34	-10	25	38.21335	2.52363	33.09149	19.27645			33.176055	19.308845
34	-10	0	-0.08657	-0.02026	-0.0831	-0.03161				
34	-10	0	-0.08988	-0.0206	-0.08603	-0.03318				

Alpha	deltac	osc	Axial	Normal	Lift	Drag	L Drift	D Drift	LIFT	DRAG
f8_[illegible]d										
22	4	0	-0.00736	-0.0025	-0.00776	-0.00044	-0.59663	0.6968		
22	4	0	31.07424	0.59169	29.03319	11.09201			29.6298233	10.3951667
22	4	0	31.08945	0.57437	29.04079	11.11377			29.6374233	10.4169267
22	4	0	30.91127	0.564	28.87171	11.05663			29.4683433	10.3597867
22	4	0	31.07087	0.56302	29.01932	11.11733			29.6159533	10.4204867
22	4	0	30.94145	0.5493	28.89418	11.08157			29.4908133	10.3847267
22	4	0	31.0912	0.5776	29.04363	11.11143			29.6402633	10.4145867
22	4	0	31.227	0.59576	29.17635	11.14546			29.7729833	10.4486167
22	4	0	30.99523	0.56749	28.95086	11.08485			29.5474933	10.3880067
22	4	0	31.37042	0.61409	29.31619	11.18219			29.9128233	10.4853467
22	4	0	31.21757	0.60439	29.17084	11.13393			29.7674733	10.4370867
22	4	0	-0.2645	-0.92306	-0.59103	0.75676				
22	4	0	-0.30388	-0.84712	-0.59909	0.6716				
22	4	0	-0.30806	-0.83864	-0.59978	0.66217				
									29.6483393	10.4150737
f8_[illegible]e										
22	4	0	-0.00143	-0.00348	-0.00263	0.00269	1.53516	0.3648		
22	4	0	31.46339	0.94538	29.52649	10.90985			27.99133	10.54508
22	4	0	31.79638	0.99772	29.85484	10.98606			28.31968	10.62129
22	4	0	31.62071	0.96382	29.67927	10.95169			28.14411	10.58692
22	4	0	31.43195	0.95912	29.50249	10.88533			27.96733	10.52056
22	4	0	31.48499	0.97408	29.55728	10.89133			28.02212	10.52656
22	4	0	31.56488	0.97123	29.63028	10.9239			28.09512	10.55913
22	4	0	31.55297	0.97294	29.61988	10.91785			28.08472	10.55308
22	4	0	31.65399	0.97173	29.71309	10.95682			28.17793	10.59205
22	4	0	31.66766	0.97714	29.72778	10.95692			28.19262	10.59215
22	4	0	31.71168	1.00152	29.77774	10.95081			28.24258	10.58604
22	4	0	1.6126	0.27167	1.59695	0.3522				
22	4	0	1.50744	0.20207	1.47337	0.37734				
									28.123754	10.568286
f8_[illegible]f										
22	4	0	-0.00358	-0.00163	-0.00393	0.00017	0.85711	0.1467		
22	4	0	30.5542	0.87734	28.65802	10.63235			27.80091	10.485665
22	4	0	30.46127	0.88843	28.57601	10.58725			27.7189	10.440565
22	4	0	30.51857	0.89769	28.63261	10.60014			27.7755	10.453455
22	4	0	30.40341	0.88334	28.52045	10.5703			27.66334	10.423615
22	4	0	30.58486	0.89828	28.69429	10.62442			27.83718	10.477735
22	4	0	30.49858	0.89809	28.61422	10.59227			27.75711	10.445585
22	4	0	30.40451	0.89508	28.52587	10.55983			27.66876	10.413145
22	4	0	30.74074	0.92427	28.84855	10.65872			27.99144	10.512035
22	4	0	30.63069	0.90929	28.74091	10.63138			27.8838	10.484695
22	4	0	0.85472	0.18191	0.86063	0.15152				
22	4	0	0.84458	0.18824	0.85359	0.14185				
									27.7885489	10.4596106

Alpha	deltac	osc	Axial	Normal	Lift	Drag	L Drift	D Drift	LIFT	DRAG
f8_7g										
22	7	0	0.0011	0.00328	0.00225	-0.00263	0.74935	0.435915		
22	7	0	31.90164	0.53137	29.77774	11.45788			29.02839	11.021965
22	7	0	31.91644	0.54683	29.79726	11.44909			29.04791	11.013175
22	7	0	31.92946	0.5402	29.80685	11.46012			29.0575	11.024205
22	7	0	32.01633	0.54447	29.88899	11.4887			29.13964	11.052785
22	7	0	31.75223	0.52617	29.63726	11.40674			28.88791	10.970825
22	7	0	31.88155	0.55147	29.76664	11.43173			29.01729	10.995815
22	7	0	31.73667	0.53483	29.62608	11.39288			28.87673	10.956965
22	7	0	31.49488	0.50331	29.39008	11.33153			28.64073	10.895615
22	7	0	31.79455	0.54468	29.68343	11.40543			28.93408	10.969515
22	7	0	31.80663	0.55473	29.6984	11.40064			28.94905	10.964725
22	7	0	0.86229	-0.12838	0.7514	0.44205				
22	7	0	0.85388	-0.11854	0.7473	0.42978				
									28.957923	10.986559
f8_7h										
22	7	0	0.00464	0.00196	0.00503	-0.00008	0.147735	0.10499		
22	7	0	31.37217	0.69388	29.3477	11.10887			29.199965	11.00388
22	7	0	31.4579	0.70042	29.42964	11.13492			29.281905	11.02993
22	7	0	31.62975	0.72285	29.59738	11.1785			29.449645	11.07351
22	7	0	31.32207	0.71252	29.30823	11.07281			29.160495	10.96782
22	7	0	31.21184	0.68765	29.19671	11.05459			29.048975	10.9496
22	7	0	31.25055	0.68913	29.23316	11.06771			29.085425	10.96272
22	7	0	31.30629	0.70282	29.28996	11.0759			29.142225	10.97091
22	7	0	31.31798	0.69745	29.29879	11.08526			29.151055	10.98027
22	7	0	31.22276	0.68233	29.20484	11.06361			29.057105	10.95862
22	7	0	31.47353	0.71185	29.44841	11.13018			29.300675	11.02519
22	7	0	0.18473	-0.04152	0.15573	0.1077				
22	7	0	0.16788	-0.04249	0.13974	0.10228				
									29.187747	10.992245

Alpha	deltac	osc	Axial	Normal	Lift	Drag	L Drift	D Drift	LIFT	DRAG
f8_7i										
22	10	0	-0.00241	0.00619	0.00009	-0.00664	0.43776	0.063985		
22	10	0	30.29243	0.01867	28.09365	11.33043			27.65589	11.266445
22	10	0	30.26281	-0.00197	28.05846	11.33847			27.6207	11.274485
22	10	0	30.34999	0.01804	28.14678	11.35258			27.70902	11.288595
22	10	0	30.31127	0.03574	28.11751	11.32166			27.67975	11.257675
22	10	0	30.16542	0.02702	27.97902	11.27511			27.54126	11.211125
22	10	0	30.5247	0.02776	28.31241	11.40902			27.87465	11.345035
22	10	0	30.19614	-0.01542	27.99159	11.32597			27.55383	11.261985
22	10	0	30.4833	0.00374	28.26502	11.41578			27.82726	11.351795
22	10	0	30.44404	0.01464	28.23271	11.39096			27.79495	11.326975
22	10	0	30.37891	0.01319	28.17177	11.36791			27.73401	11.303925
22	10	0	0.4372	0.10768	0.4457	0.06394				
22	10	0	0.42251	0.10165	0.42982	0.06403				
									27.699132	11.288804
f8_7j										
22	10	0	-0.0096	-0.00307	-0.01005	-0.00075	0.98632	0.52066		
22	10	0	29.76166	-0.12333	27.54833	11.26327			26.56201	10.74261
22	10	0	29.99974	-0.09387	27.78011	11.32513			26.79379	10.80447
22	10	0	30.18648	-0.06846	27.96277	11.37153			26.97645	10.85087
22	10	0	30.14477	-0.06979	27.9236	11.35714			26.93728	10.83648
22	10	0	30.05109	-0.07977	27.833	11.3313			26.84668	10.81064
22	10	0	29.74399	-0.11668	27.53444	11.25048			26.54812	10.72982
22	10	0	29.87518	-0.12213	27.65404	11.30467			26.66772	10.78401
22	10	0	29.94318	-0.09471	27.72735	11.30473			26.74103	10.78407
22	10	0	30.05563	-0.09924	27.82992	11.35105			26.8436	10.83039
22	10	0	29.94534	-0.09238	27.73023	11.30338			26.74391	10.78272
22	10	0	1.1182	-0.11439	0.99392	0.52495				
22	10	0	1.10089	-0.11214	0.97872	0.51637				
									26.766059	10.795608
f8_7k										
22	10	0	-0.00218	0.0063	0.00034	-0.00666	0.58517	0.20833		
22	10	0	29.0459	-0.06998	26.90467	10.94567			26.3195	10.73734
22	10	0	29.32488	-0.06396	27.16559	11.0446			26.58042	10.83627
22	10	0	29.41918	-0.0449	27.26017	11.06225			26.675	10.85392
22	10	0	29.0485	-0.07941	26.90356	10.95539			26.31839	10.74706
22	10	0	29.36942	-0.03759	27.21677	11.03683			26.6316	10.8285
22	10	0	29.53231	-0.03731	27.3679	11.09759			26.78273	10.88926
22	10	0	29.33399	-0.05674	27.17674	11.04131			26.59157	10.83298
22	10	0	29.36772	-0.04919	27.21085	11.04694			26.62568	10.83861
22	10	0	29.26748	-0.05562	27.1155	11.01536			26.53033	10.80703
22	10	0	29.34477	-0.05921	27.18582	11.04764			26.60065	10.83931
22	10	0	29.24413	-0.07476	27.08668	11.02436			26.50151	10.81603
22	10	0	29.1505	-0.07521	26.9997	10.9897			26.41453	10.78137

Alpha	deltac	osc	Axial	Normal	Lift	Drag	L Drift	D Drift	LIFT	DRAG
f8_8a										
34	-4	0	0 0009	-0.00252	-0 00066	0 00259	-0 300755	-0 388825		
34	-4	0	40 22267	1.97294	34.44936	20 85659			34.750115	21.245415
34	-4	0	39 89114	1.94119	34 15676	20 69752			34 457515	21.086345
34	-4	0	40 00079	1.95653	34.25623	20.74612			34 556985	21.134945
34	-4	0	40.00304	1.95192	34.25552	20.7512			34 556275	21.140025
34	-4	0	39 98239	1.95791	34 24176	20 73469			34.542515	21.123515
34	-4	0	39.78644	1 93615	34.06714	20 64315			34.367895	21.031975
34	-4	0	39 93771	1.9491	34 19978	20.71701			34 500535	21.105835
34	-4	0	39.79936	1.92229	34 0701	20.66187			34 370855	21.050695
34	-4	0	39 94145	1.9582	34 20798	20.71156			34 508735	21.100385
34	-4	0	39.97606	1.9509	34 23259	20.73696			34.533345	21.125785
34	-4	0	-0 47321	0.13272	-0 31809	-0.37465				
34	-4	0	-0 46032	0.17562	-0 28342	-0 403				
									34.514477	21.114492
f8_8b										
34	-4	0	0 00112	0 00033	0.00111	0.00035	0 675522	0.381124		
34	-4	0	40 50123	1.87626	34.62623	21.09251			33 950708	20.711386
34	-4	0	40 69895	1 88873	34.79712	21.19273			34.121598	20 811606
34	-4	0	40 6547	1.86863	34.7492	21.18465			34.073678	20 803526
34	-4	0	40 60938	1.8773	34.71648	21.15213			34 040958	20.771006
34	-4	0	40 36395	1.84504	34.49497	21.04163			33 819448	20.660506
34	-4	0	40.70757	1 86007	34 78824	21.22132			34.112718	20.840196
34	-4	0	40 61171	1.85734	34.70725	21.16997			34.031728	20.788846
34	-4	0	40 31008	1.83283	34.44348	21.02162			33.767958	20.640496
34	-4	0	40 40606	1.80956	34.51003	21.09459			33 834508	20.713466
34	-4	0	40 38613	1.83102	34.50551	21.06565			33 829988	20 684526
34	-4	0	0.83796	0.06411	0.73055	0 41543				
34	-4	0	0 80925	0.06238	0.70578	0.40081				
34	-4	0	0.78429	0 06304	0.68546	0.38631				
34	-4	0	0.73	0 06503	0 64157	0.3543				
34	-4	0	0.70426	0.05434	0.61425	0.34877				
									33 958329	20.742556
f8_8c										
34	-4	0	-0.00433	0 00013	-0 00352	-0.00253	0 2601	0.151165		
34	-4	0	40.25666	1.73935	34 34691	21.06925			34.08681	20.918085
34	-4	0	40 09141	1.72334	34.20096	20.99012			33.94086	20.838955
34	-4	0	40.2247	1.72195	34 31069	21.06581			34 05059	20.914645
34	-4	0	40.23239	1.72236	34 3173	21.06976			34.0572	20.918595
34	-4	0	40.15007	1.70787	34.24094	21.03574			33.98084	20.884575
34	-4	0	40 24087	1.72757	34.32724	21.07019			34 06714	20.919025
34	-4	0	40.12837	1.73277	34.23688	21.00297			33 97678	20.851805
34	-4	0	40.05269	1.68996	34.1502	20.99614			33 8901	20 844975
34	-4	0	40 18229	1.72324	34.27626	21.04102			34 01616	20 889855

Alpha	deltac	osc	Axial	Normal	Lift	Drag	L Drift	D Drift	LIFT	DRAG
f8_8d										
34	-7	0	0.0029	0.00273	0.00393	-0.00064	-0.03056	0.25898		
34	-7	0	41.05867	1.83191	35.06357	21.44099			35.09413	21.18201
34	-7	0	41.04169	1.83885	35.05337	21.42575			35.08393	21.16677
34	-7	0	41.00061	1.84751	35.02416	21.39559			35.05472	21.13661
34	-7	0	41.08687	1.86157	35.10353	21.43218			35.13409	21.1732
34	-7	0	41.03503	1.8505	35.05437	21.41236			35.08493	21.15338
34	-7	0	40.98817	1.83286	35.00566	21.40078			35.03622	21.1418
34	-7	0	40.91791	1.8479	34.95582	21.34902			34.98638	21.09004
34	-7	0	40.85591	1.81953	34.88855	21.33787			34.91911	21.07889
34	-7	0	40.93922	1.83857	34.96826	21.36868			34.99882	21.1097
34	-7	0	41.19049	1.85859	35.18778	21.49258			35.21834	21.2336
34	-7	0	0.14069	-0.24088	-0.01806	0.27837				
34	-7	0	0.1183	-0.23086	-0.03102	0.25755				
34	-7	0	0.09946	-0.22364	-0.0426	0.24102				
									35.061067	21.1466
f8_8e										
34	-7	0	-0.00396	-0.00142	-0.00407	-0.00104	0.481075	0.161965		
34	-7	0	40.81865	2.14591	35.04017	21.04645			34.559095	20.884485
34	-7	0	41.1198	2.17603	35.30668	21.18989			34.825605	21.027925
34	-7	0	41.09325	2.1627	35.27722	21.18609			34.796145	21.024125
34	-7	0	40.85238	2.15713	35.07441	21.05602			34.593335	20.894055
34	-7	0	41.06923	2.16638	35.25936	21.16961			34.778285	21.007645
34	-7	0	40.68771	2.13516	34.92561	20.98215			34.444535	20.820185
34	-7	0	40.98004	2.17203	35.18858	21.11505			34.707505	20.953085
34	-7	0	40.9968	2.14082	35.18502	21.1503			34.703945	20.988335
34	-7	0	41.05697	2.17231	35.25251	21.15784			34.771435	20.995875
34	-7	0	40.85895	2.1407	35.07067	21.07332			34.589595	20.911355
34	-7	0	0.50234	0.13466	0.49176	0.16926				
34	-7	0	0.47646	0.13482	0.47039	0.15467				
									34.676948	20.950707
f8_8f										
34	-7	0	-0.00019	-0.00109	-0.00077	0.0008	0.44318	0.24702		
34	-7	0	41.56317	2.12513	35.64578	21.48002			35.2026	21.233
34	-7	0	41.23483	2.06886	35.34212	21.34306			34.89894	21.09604
34	-7	0	41.10831	2.07755	35.24208	21.26511			34.7989	21.01809
34	-7	0	41.31058	2.08975	35.4166	21.3681			34.97342	21.12108
34	-7	0	41.12817	2.08238	35.26125	21.27221			34.81807	21.02519
34	-7	0	41.5554	2.12624	35.63997	21.47475			35.19679	21.22773
34	-7	0	41.44997	2.10485	35.5406	21.43353			35.09742	21.18651
34	-7	0	41.62684	2.11147	35.69094	21.52695			35.24776	21.27993
34	-7	0	41.30564	2.08305	35.40875	21.3709			34.96557	21.12388
34	-7	0	41.44951	2.11948	35.5484	21.42114			35.10522	21.17412
34	-7	0	41.43381	2.11353	35.53206	21.41729			35.08888	21.17027

Alpha	dellac	osc	Axial	Normal	Lift	Drag	L Drift	D Drift	LIFT	DRAG
f8_8g										
34	-10	0	0.00844	0.01712	0.01657	-0.00947	0.00405	0.1813		
34	-10	0	0.0024	-0.00284	0.00041	0.0037				
34	-10	0	40.03282	2.19241	34.41469	20.56848			34.41064	20.38715
34	-10	0	40.32609	2.24197	34.68554	20.69138			34.68149	20.51005
34	-10	0	40.05069	2.22244	34.4463	20.55358			34.44225	20.37225
34	-10	0	40.04791	2.22091	34.44314	20.55329			34.43909	20.37196
34	-10	0	40.17809	2.22976	34.55601	20.61875			34.55196	20.43742
34	-10	0	40.56853	2.26761	34.90087	20.8057			34.89682	20.62437
34	-10	0	40.49889	2.26368	34.84094	20.77001			34.83689	20.58868
34	-10	0	40.539	2.26119	34.8728	20.79451			34.86875	20.61318
34	-10	0	40.6697	2.25222	34.97613	20.87503			34.97208	20.6937
34	-10	0	40.52405	2.25634	34.85769	20.79017			34.85364	20.60884
34	-10	0	0.11281	-0.15027	0.0095	0.18766				
34	-10	0	0.09669	-0.14586	-0.0014	0.175				
									34.695361	20.52076
f8_8h										
34	-10	0	-0.00218	0.00347	0.00013	-0.0041	0.13682	0.1239		
34	-10	0	40.65121	2.33943	35.00957	20.79239			34.872755	20.668475
34	-10	0	40.07881	2.29232	34.50869	20.51136			34.371875	20.387445
34	-10	0	40.48873	2.33822	34.87419	20.70254			34.737375	20.578625
34	-10	0	40.25462	2.30787	34.66314	20.59679			34.526325	20.472875
34	-10	0	40.49042	2.35252	34.88359	20.69163			34.746775	20.567715
34	-10	0	40.41445	2.32625	34.80592	20.67092			34.669105	20.547005
34	-10	0	40.17815	2.31386	34.60309	20.54906			34.466275	20.425145
34	-10	0	40.29335	2.31648	34.70006	20.6113			34.563245	20.487385
34	-10	0	40.38095	2.35012	34.7915	20.63241			34.654685	20.508495
34	-10	0	40.30584	2.33729	34.72205	20.60104			34.585235	20.477125
34	-10	0	0.19398	-0.02678	0.14585	0.13067				
34	-10	0	0.17145	-0.02568	0.12778	0.11716				
									34.619365	20.512029

APPENDIX F: BASELINE VERIFICATION DATA

Alpha	Deltac	Osc.	Axial	Normal	Lift	Drag
f7_23a						
22	7	0	-0.00366	0.00625	-0.00105	-0.00716
22	7	0	43.22227	1.81439	40.75467	14.50907
22	7	0	43.08132	1.81535	40.62435	14.45538
22	7	0	42.96693	1.8219	40.52074	14.40646
22	7	0	43.06607	1.811	40.60858	14.45371
22	7	0	43.00628	1.84902	40.56739	14.39605
22	7	0	-3.84245	1.97197	-2.82395	-3.26778
f7_23b						
22	7	0	0.00539	-0.00016	0.00493	0.00217
22	7	0	48.87875	1.55483	45.90204	16.86869
22	7	0	48.78839	1.55381	45.81787	16.83578
22	7	0	48.73988	1.55201	45.77222	16.81928
22	7	0	48.54549	1.55417	45.5928	16.74446
22	7	0	48.52331	1.5433	45.56816	16.74623
22	7	0	4.04242	1.92216	4.46812	-0.26788
22	7	0	3.96778	1.94074	4.40587	-0.31306
f7_23c						
22	7	0	0.01158	0.01869	0.01774	-0.01299
22	7	0	-0.00142	0.00136	-0.00081	-0.00179
22	7	0	45.54404	0.7319	42.50187	16.38249
22	7	0	45.4931	0.72367	42.45156	16.37104
22	7	0	45.58084	0.74295	42.54014	16.38603
22	7	0	45.29687	0.7019	42.26146	16.31772
22	7	0	45.0858	0.69297	42.06242	16.24692
22	7	0	0.48201	0.39913	0.59643	-0.18951
22	7	0	0.47209	0.41565	0.59342	-0.20853
f7_23d						
22	7	0	-0.00318	0.00164	-0.00234	-0.00271
22	7	0	45.14908	0.9999	42.23607	15.98606
22	7	0	45.18414	0.9762	42.25969	16.02116
22	7	0	45.08298	0.98417	42.16889	15.97587
22	7	0	45.19839	0.98736	42.27709	16.01615
22	7	0	0.91205	1.31556	1.33845	-0.8781
f7_23e						
22	7	0	-0.00028	0.00085	0.00006	-0.00089
22	7	0	44.91719	0.54877	41.85206	16.31746
22	7	0	44.82931	0.53856	41.76676	16.29401
22	7	0	44.78014	0.538	41.72097	16.27611
22	7	0	44.81276	0.55827	41.7588	16.26954

22	7	0	0.41215	-0.4754	0.20405	0.59518
f7_24a						
22	7	0	0.00276	0.00114	0.00298	-0.00002
22	7	0	45.64971	0.98359	42.69413	16.18872
22	7	0	45.80381	1.01084	42.84722	16.22118
22	7	0	46.00458	1.03341	43.04183	16.27545
22	7	0	45.84045	0.99294	42.87449	16.2515
22	7	0	45.89534	0.99177	42.92494	16.27315
22	7	0	1.13744	1.24304	1.52027	-0.72643
22	7	0	1.11732	1.24617	1.50278	-0.73688
f7_24b						
22	7	0	0.00131	0.00216	0.00202	-0.00151
22	7	0	45.9755	0.63683	42.8663	16.63227
22	7	0	45.8311	0.62404	42.72762	16.59003
22	7	0	45.69937	0.61853	42.60342	16.5458
22	7	0	45.67146	0.62341	42.57938	16.53081
22	7	0	45.79478	0.62915	42.69586	16.57169
22	7	0	0.39956	0.8246	0.67936	-0.61487
f7_31c						
22	7	0	-0.00498	0.00948	-0.00107	-0.01065
22	7	0	-0.0061	0.00612	-0.00336	-0.00796
22	7	0	44.29352	1.51677	41.63642	15.18632
22	7	0	44.24351	1.53731	41.59775	15.14855
22	7	0	44.02367	1.51325	41.38491	15.0885
22	7	0	44.31361	1.54449	41.66544	15.16814
22	7	0	44.24907	1.51762	41.59554	15.16888
22	7	0	0.84917	1.5769	1.37806	-1.14397
22	7	0	0.84568	1.58478	1.37777	-1.15259
f7_31d						
22	7	0	-0.00241	-0.00009	-0.00227	-0.00082
22	7	0	45.51758	1.76652	42.86491	15.41329
22	7	0	45.66733	1.77627	43.00741	15.46035
22	7	0	46.08508	1.81421	43.40895	15.58167
22	7	0	45.65885	1.7745	42.99888	15.45882
22	7	0	45.77572	1.79078	43.11335	15.4875
22	7	0	45.69706	1.81211	43.0484	15.43826
22	7	0	1.37173	1.98313	2.01474	-1.32487
f7_31e						
22	4	0	-0.00409	0.00144	-0.00326	-0.00287
22	4	0	45.42909	1.56251	42.70645	15.5693
22	4	0	45.35989	1.53503	42.63199	15.56886

22	4	0	45.41503	1.55866	42.69196	15.56761
22	4	0	45.23514	1.5373	42.51718	15.52003
22	4	0	45.28674	1.5322	42.5631	15.54408
22	4	0	0.09442	0.3104	0.20383	-0.25243
22	4	0	0.09302	0.347	0.21624	-0.28689
f7_31f						
22	4	0	-0.00013	0.01764	0.00648	-0.0164
22	4	0	0.00261	0.02046	0.01009	-0.018
22	4	0	0.00093	0.00244	0.00178	-0.00191
22	4	0	0.0019	0.01081	0.00581	-0.00931
22	4	0	45.70637	1.56307	42.96375	15.67266
22	4	0	45.36468	1.54013	42.63835	15.56592
22	4	0	45.19558	1.52913	42.47743	15.51278
22	4	0	45.43248	1.54663	42.70364	15.5853
22	4	0	45.43199	1.55858	42.70766	15.57403
22	4	0	0.31819	0.21651	0.37613	-0.08155
f7_31g						
22	7	0	-0.00197	0.00505	0.00007	-0.00542
22	7	0	46.09751	2.26241	43.58838	15.17076
22	7	0	45.82527	2.24549	43.32962	15.08447
22	7	0	45.74109	2.2269	43.24461	15.07017
22	7	0	45.91938	2.26097	43.42268	15.10537
22	7	0	45.96782	2.25972	43.46713	15.12467
22	7	0	0.09739	0.68963	0.34864	-0.60293
f7_31h						
22	7	0	-0.00016	0.00198	0.0006	-0.0019
22	7	0	45.8176	1.30976	42.97198	15.94918
22	7	0	45.83929	1.2934	42.98596	15.97248
22	7	0	45.73742	1.2825	42.88743	15.94443
22	7	0	45.4699	1.25252	42.62816	15.87201
22	7	0	45.78298	1.28259	42.92971	15.96141
22	7	0	2.50588	0.97523	2.68874	0.0345
22	7	0	2.45943	0.98105	2.64785	0.0117
f7_31i						
22	10	0	0.00256	0.00362	0.00374	-0.0024
22	10	0	45.84462	0.86715	42.83123	16.36969
22	10	0	44.99778	0.80006	42.02093	16.11467
22	10	0	45.23752	0.80734	42.24593	16.19772
22	10	0	45.36601	0.84841	42.38045	16.20777
22	10	0	45.0211	0.81808	42.04929	16.10669
22	10	0	45.47394	0.84321	42.47857	16.25302
22	10	0	45.3379	0.86152	42.3593	16.18509

22	10	0	0.76737	0.68249	0.96716	-0.34533
f7_31j						
22	10	0	-0.00484	-0.00298	-0.0056	0.00095
22	10	0	43.86147	0.15559	40.72593	16.28654
22	10	0	44.08762	0.18305	40.9459	16.34579
22	10	0	43.79933	0.17162	40.67432	16.24839
22	10	0	44.07719	0.18537	40.9371	16.33973
22	10	0	43.78001	0.15706	40.65095	16.25465
22	10	0	-0.1228	-0.4055	-0.26576	0.32997
f7_31k						
22	7	0	0.00841	0.00364	0.00916	-0.00023
22	7	0	47.31729	1.38383	44.39022	16.44231
22	7	0	47.44788	1.42378	44.52627	16.45418
22	7	0	47.56302	1.42304	44.63275	16.498
22	7	0	47.57654	1.40812	44.63969	16.5169
22	7	0	47.33187	1.38893	44.40565	16.44303
22	7	0	3.01299	0.68643	3.05073	0.49224
22	7	0	2.9889	0.68428	3.0276	0.48521

INITIAL DISTRIBUTION LIST

1.	Defense Technical Information Center Cameron Station Alexandria, VA 22304-6145	2
2.	Library, Code 52 Naval Postgraduate School Monterey, CA 93943-5002	2
3.	Professor Daniel J. Collins, Code AA/Co Chairman, Department of Aeronautics and Astronautics Naval Postgraduate School Monterey, CA 93943-5000	1
4.	Michael J. Harris Code AIR-530TA Naval Air Systems Command Washington, DC 20361	1
5.	Professor Richard M. Howard, Code AA/Ho Naval Postrgrduate School Monterey, CA 93943-5000	2
6.	Professor Louis V. Schmidt, Code AA/Sc Naval Postrgrduate School Monterey, CA 93943-5000	2
7.	LT Dean C. Schmidt 100 Cuesta Vista Dr. Monterey, CA 93940	2

Thesis
S33716 Schmidt
c.1 Lift enhancement using
a close-coupled
oscillating canard.